Accurate AVO modelling and reservoir characterisation of the Upper Cretaceous deepwater reservoirs in the Vøring Basin

Bruce Chalmers

Thesis submitted in partial fulfillment of the requirements of the Robert Gordon University for the degree of Master of Philosophy

September 2017

Abstract

In an exploration setting, reservoir characterisation is concerned with the identification of fluids and lithology. Seismic interpreters seek to distinguish hydrocarbons from brine and sand from shale. Amplitude vs offset (AVO) is a fundamental technique used for this purpose. AVO occurs when seismic sound waves encounter compressible Gas or Oil which reduces the compressional velocity or P-Velocity of the rock. Other properties, such as high porosity, can also cause an AVO effect similar to that of a hydrocarbon response. Therefore, AVO effects need to be accurately modelled before prospects can be drilled. The aim of this study is to apply AVO and other reservoir characterisation techniques to five wells from the Vøring Basin. In doing so, it can be established which of the techniques are most accurate in an exploration setting. The Vøring basin is an area dominated by deep-marine reservoirs which are a major play in oil and gas exploration. The acquired wells, three of which are dry wells and two of which are gas discoveries, targeted Upper Cretaceous reservoirs formed by deep-marine slope and submarine fan type environments (Morton et al. 2004). The associated facies vary from thick sheet sands to thin channels and shale rich lobes (Goodall et al. 2002). Avseth et al. (2011) suggest that geological data from wells can be linked to the seismic response and AVO using rock physics models whereas Connolly (1999) and Florez and Kuzmin (2015) propose a different approach which links geology to seismic through the use of impedance. This study aims to compare and contrast the forward modelling approach outlined by Avseth et al. (2011) and Simm and Bacon (2013) with that of the impedance approach from Connolly (1999) and Florez and Kuzim (2015). The initial part of this study is concerned with the interpretation of the raw well data. This enables a number of modelling steps to be applied. The results produced for each well are then compared using different plots or synthetic seismic models. In this study, the results obtained show several of the techniques provide a convenient way to discriminate fluid and lithology or estimate the seismic response but few, with the exception of Acoustic Impedance vs Gradient Impedance, cater for both needs. Traditional AVO classification does provide a basic understanding of the amplitude behaviour but is insufficient to completely discriminate hydrocarbons from brine. This reinforces the many studies that suggest that AVO cannot be relied upon as definitive direct indicator of hydrocarbons (DHI). Furthermore, the results of this study show that traditional AVO classification must be supplemented with additional steps such as stochastic modelling or fluid substitution, to be more effective at distinguishing hydrocarbons from brine. This study emphasises the need to take an integrated approach paying attention to key geological factors that influence reservoirs in a setting such as deep-water.

Reservoir Characterisation, AVO, Geophysics, RockPhysics, Vøring Basin

Acknowledgments

Thanks goes to Prof. Babs Oyeneyin for motivating and challenging me through the research. Colleagues Ole Johannes Rossebø and Prof. Arild Buland for their help in getting started. Thanks also goes to my parents Robert and Cynthia for their support. Finally my wife Helene and baby Nikolas, thanks for always being there to help.

Declaration

I declare that the work presented in this thesis is my own, except where otherwise acknowledged, and has not been submitted in any form for another degree or qualification at any other academic institution. Information derived from the published or unpublished work of others has been acknowledged in the text and a list of references is given.

Bruce Chalmers

Contents

List of Tables

List of Figures

Chapter 1

Background

This chapter introduces the main background concepts that relate to the motivation and methods used in this study. To begin with, the motivation for this study is discussed through a section outlining how seismic data is acquired and how it can be used for fluid and lithology prediction. Then, techniques and approaches for fluid and lithology prediction are discussed. Afterward a summary of the main research aims and questions are described. This is followed by a section outlining the data that was used in the study. Finally, this chapter is concluded by a conceptual plan, an outline of the thesis and a summary of the deliverables and contributions to knowledge.

1.1 Reflection Seismic Acquisition

Seismic data is acquired via the recording of sound wave reflections as they propagate through the earth. A sound or pressure wave is produced by a land or marine source and propagates down into the subsurface. When the wave encounters a boundary between two rock formations, with significant differences in their physical properties, part of the sound wave is reflected. These reflections are then recorded over a wide area as the source and receivers move. Once recorded, the reflections are plotted against travel time, to build up a picture of all the boundaries in the subsurface. The nature of the reflections are used to interpret broad geological structures as well as potential hydrocarbon traps and reservoirs.

The strength of the reflections is also an important measure of the contrast of two key properties, the compressional velocity or P-Velocity (Vp) and Density (Rho) between layers. Combined, these two terms are known as acoustic impedance (AI) and therefore seismic reflections are a direct measure of the acoustic impedance contrast between layers. The scale of the AI contrast between these layers is usually expressed by a single measurement

known as the reflection coefficient. This is equal to the scale of the difference in AI between layers.

When sound wave reflections are at an angle to a reflected point, a shear wave velocity or S-Velocity (Vs) is produced. Again, the scale of the contrast between layers controls the amount of energy that is reflected.

Seismic data is created when all the reflections are recorded. A reflection of each boundary in the subsurface is recorded, but since the method uses sounds waves, a continuous signal known as an amplitude is produced. This amplitude will return both a positive and negative response depending on the acoustic impedance contrast between layers.

Seismic reflections or amplitudes can also be grouped together as a function of incidence or offset angle with respect to a given point. This technique has traditionally been used to aid interpreters of seismic data as certain features may be clearer on a particular range of offset angles or it may reduce noise. Typically, this is done to produce seismic data grouped at Near, Mid and Far offsets. Figure 1.1 is a schematic showing how sound waves are transmitted and reflected during seismic acquisition.

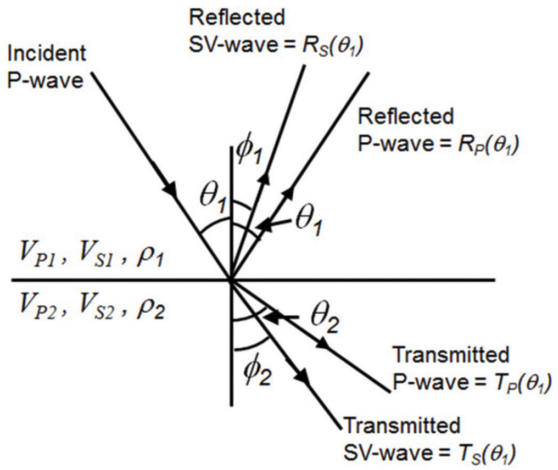

Figure 1.1: Seismic reflection and transmission from Russel et al. (2006)

Dividing seismic data into groups of offset angles led to the observation that certain amplitudes can change significantly with offset (Castagna, Swan and Foster 1998; Westphal Stephensen et al 2013). This phenomenon is known as amplitude variation with offset or AVO. All amplitudes have a AVO effect, but some, particularly gas bearing sands, can have a very strong amplitude change with offset. This observation led to the idea that AVO was a direct indicator of hydrocarbons(DHI). However, many documented cases have shown

that lithological effects can also cause AVO (Simm and Bacon 2014; Sams 1998). Analysis of seismic data angle stacks is the usual method for understanding and predicting AVO. Since many different angle stacks can exist, interpreters usually process the different angle stacks into two main products. These are known as the Intercept, which is the amplitude at zero offset and the Gradient which is the measure of changes across the angles stacks. These two measurements are a fundamental description of AVO.

Due to many AVO related failures, it is increasingly important to relate observations in the seismic to detailed lithological information from well data. Wells penetrate the subsurface and take detailed measurements of the rock formations in the form of wireline logs. These logs provide detailed information about the lithology, density, velocity and other properties albeit in a very narrow lateral range. Well data can also be modelled to produce a synthetic seismic model which is a simple reflection model based on building layers of different acoustic impedance. Firstly, a model of reflection coefficients can be calculated from the log data to estimate the contrast between each layer. This reflection model can then be convolved with a wavelet, simulating a continuous sound wave, to produce a synthetic seismogram or synthetic. In the simplest form a zero-incidence synthetic is produced from acoustic impedance which is the product of Vp and Rho. However, in order to calculate offset reflectivity S-Velocity (Vs) is required in addition. Typically these three properties (Vp,Vs,Rho) are grouped together and often to referred to as the elastic properties of a rock. By modelling different offsets for example 0 to 30 degrees, the change in amplitude or AVO can be calculated. This can then be further simplified into the two measurements Intercept and Gradient.

Naturally this allows the wells to be matched or tied to the seismic data which can build an understanding of how different lithological properties relate to amplitudes in the seismic. The well data can also be modified to produce certain scenario based models for example, different porosities or fluids. A synthetic can then be created for each of these models to estimate how the seismic data might behave under different scenarios. This process is known as forward modelling.

Different methods exist for forward modelling of different properties but typically require the input data given in elastic parameters, for example bulk modulus (K) and shear modulus (mu). Therefore the data is often transformed from Vp,Vs and Rho, and modeled in the elastic parameter domain then transformed back. Each time a new set of Vp,Vs and Rho logs are created from which a new synthetic or Intercept and Gradient can be created.

1.2 AVO and Quantitative Interpretation

Seismic interpretation is usually concerned with mapping structures for prospect identification and volumetrics. Quantitative interpretation is a branch of seismic interpretation which is more aimed at the estimation of reservoir properties from seismic. AVO is the most basic and widely used technique for quantitative interpretation (Avseth et al 2005).

In many cases AVO can be a reliable indicator of hydrocarbons. However, there are also many occasions when it can occur due to lithological and other effects. These AVO effects or anomalies are typically of interest to interpreters as they are provide a quick method for regional screening and prospect identification. In addition using AVO together with fluid and lithology modelling techniques can be useful for the analysis and risking of prospects. Naturally this makes AVO an attractive technique, as it can be a quick and easy way to identify prospects. However, subsequent AVO modeling will be required to diagnose the true cause of the observed AVO effect.

Should an AVO effect be modeled and directly linked to hydrocarbons, the seismic may then be able to directly map out the reservoir facies or even distinguish fluid contacts. Through the modeling and analysis of different scenarios, an interpreter may be able to link further geological properties to seismic observables i.e. porosity.

In general, there is also a trend in modern exploration to try to extract as much information as possible out of seismic data. Advances in seismic acquisition and processing provide higher quality data, for conducting AVO analysis, than was previously available.

1.3 AVO Classification

Understanding the link between fluids, lithology and the seismic amplitude is a key process in reservoir characterisation. One of the most basic strategies is to classify seismic amplitudes based on their AVO response. This technique relies upon classifying amplitudes into a simple qualitative scheme which identifies the reflection characteristic between two layers.

A classification scheme for AVO was first introduced by Castagna et al. (1998). The scheme woks by classifying the AVO response by a function of Intercept plotted against Gradient. From the scheme it can be observed that Intercept and Gradient can be both positive and negative. The main distinction between a positive and negative Intercept relates to the relative impedance between the two layers. If a layer is surrounded by rocks of lower impedance it will have a positive response for the Intercept. Similarly, if a low impedance layer is surrounded by high impedance layers, for example a gas sand

surrounded by shales it will give a negative Intercept.

Gradient, however, is primarily influenced by Vs changes between the layers. Negative Gradients are associated with a positive Vs contrast i.e. an increase in Vs whereas Positive Gradients are associated with a decrease in Vs (Simm and Bacon 2014).

Figure 1.2 shows the AVO Classification scheme introduced by Castagna et al. (1998). In many cases this technique has been found to improve the identification of hydrocarbon bearing sands, however, it has also resulted in ambiguous results particularly in the case of high porosity brine sands(Sams 1998; Simm and Bacon 2014).

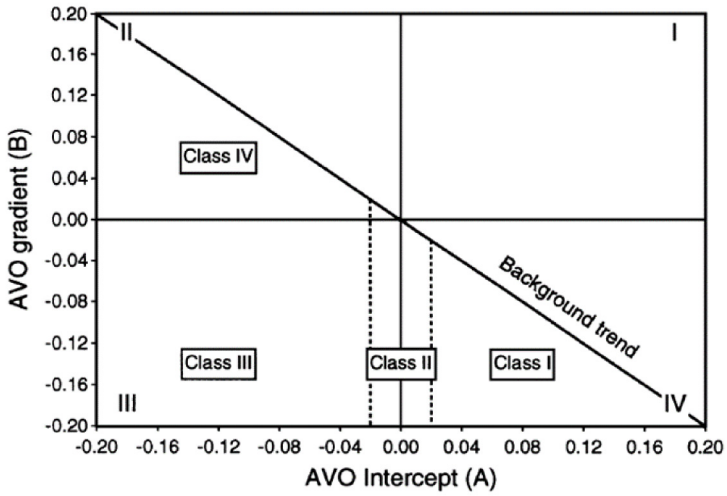

Figure 1.2: AVO classification scheme from Castagna et al (1998)

One of the biggest ambiguities in AVO classification rises from the Class II and Class III distinction. Both classes can be represented by a negative Intercept and negative Gradient, but are defined by the magnitude of the AVO effect. Sams (1998) showed that it is possible for lithological changes and not only fluids that can result in large changes in offsets. In addition it has been observed by many authors that under certain conditions, a highly porous brine sand could appear more anomalous i.e have a stronger AVO, than a less porous hydrocarbon bearing sand (Simm and Bacon 2014, Avseth et al. 2005).

Avseth et al. (2005) suggest that ambiguities arising from AVO interpretation require a more in depth analysis of the rock physics and rock micro-structure. They propose that by modelling changes in elastic properties though the use of rock physics models, a better estimation of the AVO can be made. A major challenge of this, however, is understanding the degree to which different rock properties influence the elastic properties (King 2009).

Techniques for modelling the AVO response from well data are an important way to cross reference and predict the expected amplitude response under different conditions. Application of the Gassman equation is commonly used to simulate the response of different fluids in place (Berryman 2009). Gassman fluid substitution is however, highly sensitive to porosity and dependent on having intricate knowledge of the mineral and fluid properties (Simm 2007). This Gassman equation also requires the elastic properties (Vp,Vs,Rho) to be transformed into elastic parameters like bulk and shear modulus (K and Mu). This requires different methods to estimate the Bulk and Shear Modulus of the rock, which may be a mixture of different minerals like quartz and clay. Naturally different methods existing for mixing based on the rock type which adds to the complexity of the process.

Physical properties such as porosity can be modeled using an appropriate rock physics model, that has been calibrated to the rock types of a particular study (Avseth et al. 2000). There have been many successful examples of this methodology (Avseth et al. 2000; Chi and Han 2009; Gupta et al. 2012) but it normally requires that the model has a very good fit to the input data and requires extensive knowledge of the rock texture. Properties that are required to make the process work such as depositional porosity and sorting can be difficult to estimate from raw well logs.

Regardless, all these steps can be combined together to build up a set of different scenarios which can be compared with the seismic data. The following image shows how a typical forward modelling study can be used to test different scenarios. Figure 1.3 shows how forward modelling can be applied and then compared with the seismic data.

Connolly has suggested an alternative methodology for fluid and lithology prediction based on AVO and elastic impedance theory (Connolly 1999; Whitcombe et al. 2000). This method, based on elastic properties, provides a strong link between seismic and well data in order to predict fluid or lithology. This differs from the approach by Avseth et al. (2000) as it is not an explicit forward modelling approach.

Together, all these techniques aim to help interpreters understand the amplitude behaviour or AVO which in turn can help in the identification of lithology and fluid. The purpose of this study is to evaluate which of these techniques proves the most practical when addressing a typical deepwater setting from the Vøring Basin. The different techniques are also preferred by different authors and have been developed at different times. Part of this study is to evaluate them together and conclude if they can be used together in an integrated way.

For the present study, the Vøring Basin area was selected. This area was selected as it is an active area for current and future exploration. Several wells have been drilled in this area, but it has not been as extensively drilled as other parts of the Norwegian Continental

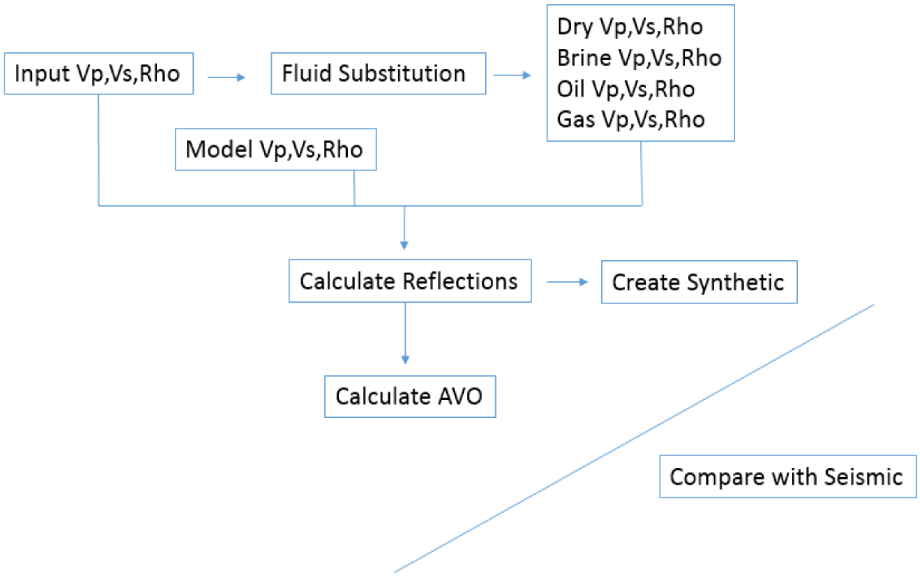

Figure 1.3: A typical Forward Modelling workflow

shelf. The Vøring Basin is a significant basin offshore Norway found West of Mid Norway in the Norwegian Sea. Several oil and gas discoveries have been made in the Vøring basin including the Luva discovery, now called the Asata Hansen field. The reservoirs associated with these discoveries were formed in a deep marine depositional environment. These types of deposits are common in oil and gas exploration and such further understanding of the characteristics of these types of reservoirs is desirable.

1.4 Research Questions, Aims and Objectives

The overall aim of the project is investigate an accurate methodology for reservoir characterisation based on AVO, lithology and fluid prediction. After a thorough interpretation of the raw well data, several modelling techniques will be applied. These techniques will be evaluated for their ability to improve the understanding of the AVO response, predict fluid or lithology and honor geological variation. By using several diverse wells from the Vøring Basin as estimation of the accuracy of each of these techniques can be understood.

Conducting a reservoir characterisation study prompts the following research questions:

1. Do the reservoir rocks from the Vøring Basin exhibit consistent AVO / elastic behaviour?

2. To what extend does the geological environment influence the elastic properties of the rocks?

3. How effective are current methods to model changes in elastic properties?

4. How to better distinguish hydrocarbon bearing sands from non-reservoir using AVO modelling techniques?

1.5 Conceptual Plan

The following steps below identify the conceptual plan for the project.

1. Conduct Geological interpretation to identify and understand reservoir rocks

2. Conduct analysis of reservoir rocks to investigate trends and behaviour

3. Model and understand Seismic and AVO response of rocks

4. Investigate forward modelling techniques for predicting fluid and lithological changes

5. Investigate impedance techniques for predicting fluid and lithology effects

6. Evaluate the benefits and limitations of each of the techniques

1.6 Thesis Outline

The thesis is divided into the following chapters

1. Introduction - To raise research questions and outline objectives

2. Background Theory- Discuss the background theory of AVO, forward modelling and impedance techniques

3. Methodology - Outline the research methodology and work plan

4. Geological Setting - Outline the geological context of the study area

5. Results - Outline the results of the study

6. Discussion and Conclusions - Present the findings and make recommendations for further work

1.6.1 Deliverables

The first step of the project is to conduct a geological interpretation of the raw data to build an understanding of the reservoir properties, using the techniques outlined in Section 3.1.

In this step several calculated logs will also be produced from the raw well data. This includes transforming raw measured logs into interpretation logs, such as Water Saturation, Facies and Porosity

The next objective, Section 3.2, is to produce a understanding of the seismic properties and AVO analysis of the reservoir zones. This builds an understanding how the raw well data behaves.

Section 3.3 outlines the forward modelling steps in which the raw data is modeled to show how the data responds to changes in fluid and lithology. This will primarily generate new data which will then be transformed into a reflectivity or AVO plot, from which a comparison can be made with the original data.

Section 3.4 outlines the impedance workflow for fluid and lithology prediction. The outcome of this will be plots in which fluid or lithological changes can be interpreted.

1.7 Contributions to knowledge

The following section describes the original contributions to knowledge made by this study.

1.7.1 Stochastic modelling of AVO

The present study proposes a stochastic approach to AVO modeling to improve understanding of the range of possible scenarios. A simple model of AVO using an average value for overburden and reservoir is not a very accurate estimate of the AVO as it does not encompass the full variability in the data. In addition applying a qualitative scheme, such as AVO classification, on a single value can result ambiguous results. This study proposes a stochastic approach based on a covariance matrix of Vp,Vs and Rho and generation of random samples from a prior distribution. This proved a more effective technique as it allowed the full range of possible AVO estimates to be plotted. The prior estimation allows the full range of the data to be incorporated into the random sampling. The extents of the output results also helps with the classification, as an estimation of probability can be made on the classification allowing uncertainty to be explored. The following figure shows an example of reflectivities calculated for a set of random samples for three different combinations of sand and shale.

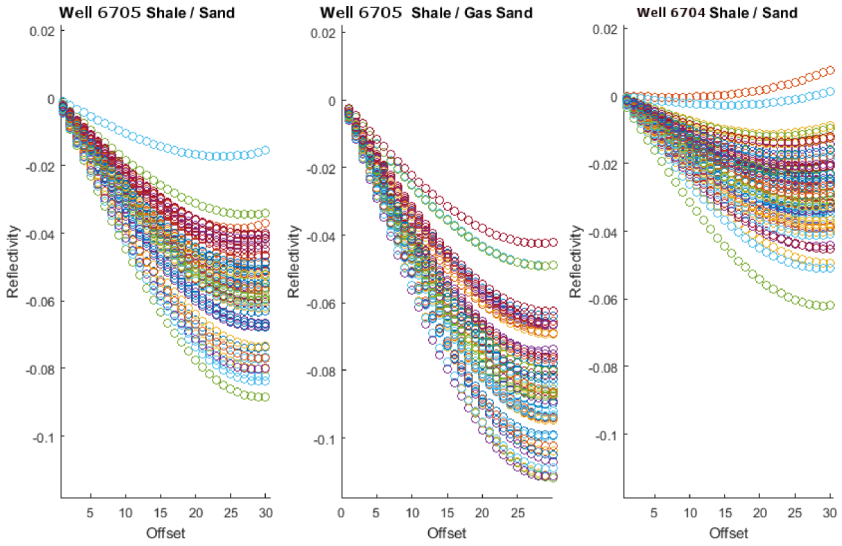

Figure 1.4: Stochastic Reflectivities

1.7.2 Impedance Cross plots and reservoir characterisation

This study highlights the use of impedance plots in reservoir characterisation. Many of the techniques used in this study could be used to either model the seismic response or predict reservoir properties, few cater for both needs. Cross plotting AI vs GI however, provides a method to relate changes in Intercept and Gradient directly to the data points. These points can also be coloured by any property i.e. porosity or water saturation allowing geological properties to be linked to changes in Intercept and Gradient, assuming there is a clear trend or separation in the data points.

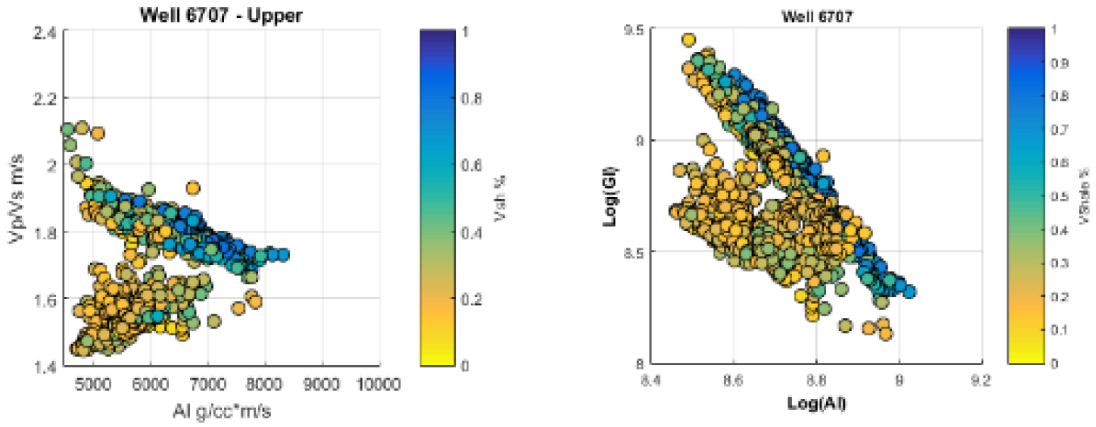

Figure 1.5: Figure showing a plot of Vp/VS vs AI and AI vs GI for Well 6707

1.7.3 Integrating Rock Physics, Impedance and AVO

Highlighted in this study is the need to take an integrated approach to AVO analysis and reservoir characterisation. It is essential to work all the way back from petrophysics and log prediction, though geological interpretation and into modelling and synthetics. This allows the interpreter to have a better understanding of the assumptions that underpin the interpretation throughout.

The first example of this is use of the fluid substitution and recalculation of AVO. Fluid substitution is commonly used to estimate the response of the seismic by varying the fluid content. In this study the results of fluid substitution were fed back into the AVO classification scheme. Since fluid or lithological effects can cause overlaps in the AVO classification scheme it was useful to estimate the change in AVO effect by changing fluid alone. This process helped to identify a background trend of brine saturated rocks, with different shale volume and porosity. This helped with the calibration of all AVO responses and helps the interpreter understand how anomalies would appear against this background trend.

In addition by integrating techniques such as Vp/Vs vs AI and AI vs GI plots interpretation of fluid and lithology can be improved. These two techniques are favoured by different authors but are used for different purposes. The previous section highlights the use of AI vs GI plots for AVO interpretation. Although a convenient way to link properties to AVO, data on this plot tends to not separate out as well as it does on a plot of Vp/Vs against AI. The strength of Vp/VS vs AI on the other hand is the ability to separate out

data in distinct clusters. For example the separation of hydrocarbons from brine sands aids the interpretation of the facies. However the downside of this plot is that it does not help to estimate the seismic response. This shows that by combining these two techniques a better understanding of how geological properties link with the AVO response can be made.

1.7.4 Modeling of deep marine geology

This study contributes to the existing understanding of deep marine reservoirs and how they can be modeled effectively. Primary variation in this type of geological setting are linked to the depositional energy which can vary between thick channel sands, to shalier more distal lobes and overbank deposits. Firstly the classic Neu-Den was an effective technique at separating out the good and poor reservoirs from a geological perspective. Plots of Vp/Vs against AI were useful for separating out further hydrocarbons from brine. When combined with a rock physics model for guidance, porosity trends could also be effectively understood using this method.

The seismic and AVO modelling shows that the deep marine reservoirs of the Vøring basin, fit with the original AVO theory. Hydrocarbon and brine sands plotted as typical Class II and Class III AVO with the gas bearing sands plotting further away from the background trend. This study shows that AVO is an effective technique for classifying these types of reservoirs but care must be taken with definition of a background or brine trend.

Fluid substitution effectively modeled changes in fluid saturation and was correctly controlled by the stiffness or porosity of the sands.

Chapter 2

Background Theory

This chapter outlines the main theory behind AVO and the geological effects that can influence seismic reflections. In addition, this chapter discusses the main techniques used to interpret AVO, model seismic and investigate other controls on rock properties.

2.1 Geological Effects on AVO

The AVO classification scheme for seismic reflections which has typically been most successful in clastic (sand and shale dominated) depositional environments. In these environments there are many factors which can influence the physical properties of the rocks and the corresponding seismic reflection. The following section outlines the main controls on the variation of reflections across the scale of a seismic survey, depositional area or basin.

2.1.1 Lithology

Understanding lithologies or facies in the study area is an important step in any reservoir characterisation study. Avseth et al. (2000) suggest that establishing a link between facies and seismic amplitude makes it possible to interpret the depositional system and further map out the seismic facies.

The reservoir properties of a single sand can vary significantly over the area of a field and even more so over a basin. Typically sands can be influenced by a number textural effects inducing sorting and roundness of the grains which are linked to the energy at time of deposition (Sain, Mavko and Mukerji 2009). These processes in turn, influence the grain contacts and pore space of the rock as its gets compacted and becomes solidified. In

addition under certain burial conditions there may be an occurrence of a cement between grains which influences the stiffness and may reduce porosity.

Clay or shale volume of a sand may also be highly variable, again due to changes in the depositional environment. For example, channel sands of a deep marine environment may contain mostly coarse sand, whereas overbank or fan deposits, which are lower energy, may contain higher amounts of shale and clay. Some depositional systems are also laminated, meaning that the environment varies between depositing sand and shale. This may be cyclic or seasonal as the depositional system changes frequently between lower and higher energy. Naturally the shale content of a rock will have an influence on the elastic properties and AVO response.

During burial rocks are subjected to mechanical compaction which in general decreases porosity with depth. This process dominates the lithology of a rock until the temperature due to burial reaches 70 degrees or higher. At temperatures above 70 degrees chemical diagenesis occurs and sands can begin to become cemented by fluids containing clay minerals. This process stiffens up the rock microstructure significantly and makes the sands less prone to further compaction. Shales are not stiffened significantly by cementation and generally become more compacted with depth and less porous (Lang 1994). This results in a crossover of the properties of sand and shale versus depth. At shallow depths sand generally has a lower impedance than shale. However, at larger depths, below where chemical compaction and cementation begins, sands can have a higher impedance than shales due to the increased density of the rock. Ramm and Bjorlykke (1994) showed that sands from the North Sea and Norwegian Sea are dominated by mechanical compaction down to depths of 2.5-3.0km. At these depths porosity is mostly influenced by the compaction, primary or depositional sorting and clay content. At greater depths, however, the biggest control on the porosity is chemical compaction and quartz cementation. All the reservoirs of the study area are around or greater than a depth of 3km and likely influenced by chemical compaction and cementation.

2.1.2 Fluid

Differing fluid fills have a significant effect of on the Vp of a rock. When a rock is saturated with gas rather than brine, the Vp will be effected, as compressible gas reduces the bulk modulus. Therefore, the effect of replacing brine with gas or oil is to reduce the acoustic impedance. However, this can be offset by the compressibility and stiffness of a rock itself. The stiffness of a rock determines how much it will be influenced by fluid content. Stiff rocks change less with the replacement of fluids where as soft rocks can change significantly

(Simm 2007).

Compared to Vp, Vs is much less sensitive to changes in fluids and hence why the Vp/Vs ratio is an important measurement which can help in the detection of fluids.

Typically, seismic reflections of a gas sand surrounded by higher impedance shales will be negative and become more negative with offset. This relates to the Class II AVO response. Naturally a brine sand surrounded by higher impedance shales may have a similar response, but will be less negative.

2.2 AVO Modelling and Analysis

2.2.1 Reflectivity

Using the Aki Richards approximation 2.1 of the Zoeppritz equation it is possible to calculate the reflectivity between two layers. Using sets of Vp,Vs and Rho, the reflection coefficient is calculated as the difference in reflectivity between layers (Fan and Ma 2011; Adeoti et al. 2015). In this case the Aki Richards approximation can calculate reflectivity for a range of offset angles.

$$Rpp(\Theta) = \frac{1}{2}(\frac{\Delta Vp}{Vp} + \frac{\Delta Rho}{Rho}) + \frac{1}{2}[\frac{\Delta Vp}{Vp} - 4\Upsilon^2(\frac{\Delta Rho}{Rho} + 2\frac{\Delta Vs}{Vs})]\Theta^2 \tag{2.1}$$

2.2.2 Amplitude versus Offset plot

A typical way to visualize the results of the Aki Richards equation calculation is to construct an Amplitude vs Offset plot. This is a plot where amplitude is on the Y-Axis and Offset is on the X-Axis. This plot shows the magnitude of a reflection at 0 incidence and how it changes as the offset angle is increased. This is the most basic way of interpreting AVO.

Two elements are important when classifying results in this type of plot, firstly if the amplitude is, at zero incidence, positive or negative. This signifies the change in acoustic impedance across the layer. If negative, there is a decrease in acoustic impedance and if positive there is an increase in acoustic impedance.

The second element is the rate of change of the reflection with offset or Gradient. All amplitudes change with offset due to increasing amounts of Vp reflectivity at higher offsets. However, the rate of change in respect to the normal incidence amplitude has been linked to the presence of hydrocarbons and can be a useful classification tool.

2.2.3 Shuey's Equation

The Shuey approximation allows the direct estimation of Intercept (2.2) and Gradient (2.3) from a reflectivity calculation. Shuey is a approximation of the Aki and Richards equation (Shuey 1985). The Shuey equation is available as a 2-term or 3-term approximation. It is generally accepted that the 2-term approximation is accurate when modelling angles of the near to mid range (Simm and Bacon 2013).

$$R(0) = \frac{1}{2}(\frac{\Delta Vp}{Vp} + \frac{\Delta Rho}{Rho}) \tag{2.2}$$

$$G = \frac{1}{2}\frac{\Delta Vp}{Vp} - 2\frac{V_s^2}{V_p^2}(\frac{\Delta Rho}{Rho} + 2\frac{\Delta Vs}{Vs}) \tag{2.3}$$

2.2.4 Intercept and Gradient / AVO Classification

Once calculated using Shuey's Equation, the Intercept and Gradient can be plotted in a cross plot of Intercept versus Gradient similar to that in figure 1.2. What is notable about this plot is that it can have both positive and negative Intercept and Gradient. This plot gives rise to the well known AVO classification scheme from Castagna et al. (1998).

2.2.5 Synthetics and Convolution

A simple synthetic seismic model can be produced from the reflection coefficients of a series of layers. Vp,Vs and Rho is used to produce an AI log which is then converted into a reflection series of positive and negative reflection coefficients. A wavelet is then convolved with this series and summarized into a single trace. This is then done at various angles of incidence for example, between zero and thirty, to produce a simple amplitude with offset synthetic. Figure 2.1 shows a plot of the data points that comprise a 25hz zero phase wavelet in a plot of amplitude against time. This wavelet was created using a wavelet toolbox in Matlab. The wavelet is considered zero phase when the peak amplitude is at time equal to zero. The type of wavelet is known as a Ricker Wavelet, this refers to the shape of the wavelet with the large positive peak and negative side lobes. This wavelet is a broad approximation of a seismic wave.

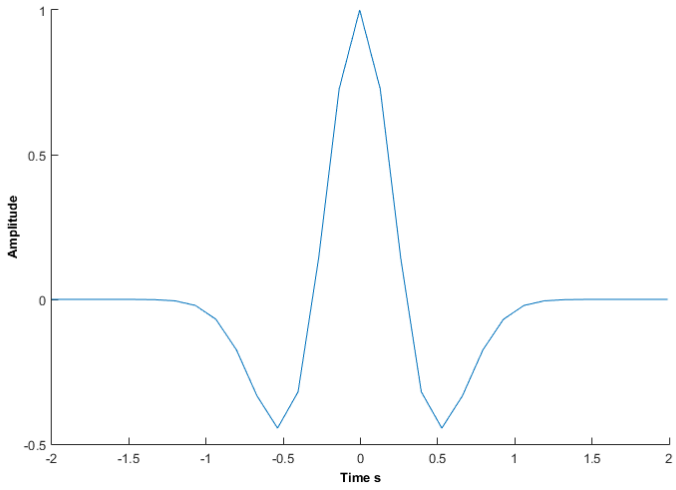

Figure 2.1: 25hz Ricker Wavelet

2.3 Fluid Substitution and Analysis

Fluid Substitution is the process of theoretically replacing the fluid content of a rock with another type of fluid. This process can be a useful way of understanding how fluid influences the seismic. In practice the application of fluid substitution usually concerns the use of the Gassmann equations, (Gassman 1951), which is also documented by Simm (2007) and Berryman (2009). This equation is used to modify the elastic modulus of the rock by first taking out the initial fluids and then substituting new fluids in. The process of fluid substitution also requires a number of different methods to prepare data for fluid substitution. This includes the Voight, Reuss and Hill methods to calculate bulk and shear modulus for mixtures of two minerals. Interpretation logs such as Water Saturation and Porosity are also required for fluid substitution.

The process of Fluids Substitution using the Gassman Equation is detailed in Appendix B.

2.3.1 Mixing

The Gassman equation requires an estimation of the bulk and shear modulus of the rock. These values are typically calculated using methods to estimate the bulk and shear modulus from proportions of minerals i.e. quartz and clay. Various methods exist for mixing these minerals together including Voight, Reuss and Hill Average. Figure 2.2 shows the bulk

modulus calculated for a quartz and clay mixture based on different methods. Typically, for clastic reservoirs, a VShale log is used to estimate the proportions of quartz and shale.

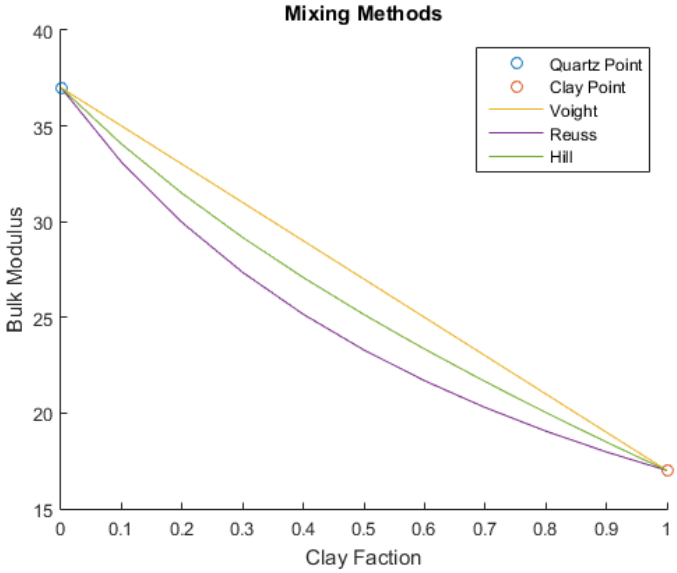

Figure 2.2: Mixing Methods for calculating the Bulk Modulus of a two mineral rock

The Voight and Reuss bounds indicate the maximum and minimum possible bulk modulus for a mixture of the two grains in a rock. The Hill Average, Hill (1951), represents and average of these two bounds. The Hill Average is seen as a sufficient for most uses, however certain textural characteristics of the rock many prompt use of a different mixing method.

2.3.2 Calculating Fluid Effects

The Gassman Fluid Substitution equations are sensitive to certain input parameters and hence quality control is an important process. Once such method suggested by many authors including Simm (2007) is to produce a plot of Kdry/Kmin (Dry Shear Modulus / Mineral Bulk Modulus) vs Porosity. The plot of Kdry/Kmin, also known as normalized bulk modulus, vs porosity can be useful for identifying which rocks will be sensitive to fluid changes and which will be less sensitive. Lines representing constant normalized bulk modulus can be added in addition, to annotate the plot. Normal stiffness brine or hydrocarbon saturated rock should lie within these bounds. Rocks with a low Kdry/Kmin value are considered soft where as high values of Kdry/kmin are considered stiff.

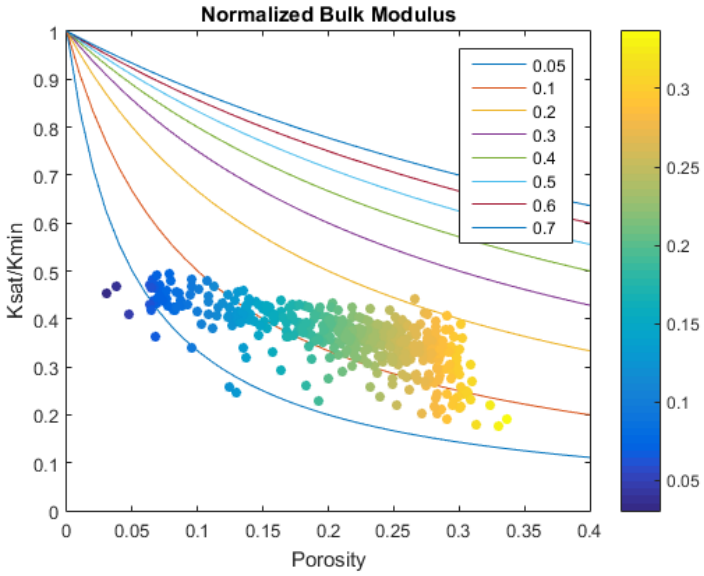

Figure 2.3: QC plot of Normalized Bulk Modulus

2.4 Rock Physics Models

Rock physics models are empirical and model based templates which are based on laboratory measurements of different rock properties. These models can be used as simple overlays to well data to aid interpretation, or can be used to model data based on certain conditions.

2.4.1 Gardner

Gradner's Model (2.4) is a model proposed by Gardner et al. (1974) which describes the relationship between density and velocity for different lithologies.

This model is an empirical model which is most commonly used to derive Vp or Vs from density. The Gardner equations can be calculated for shale and sand using different factors detailed in the table below.

$$Rho = a \times Vp^{b} \tag{2.4}$$

Table 2.1: Gardner's equations factors for different lithologies from Gardner et al. (1974)

Lithology	a	b
Sand	1.66	0.261
Shale	1.75	0.265

2.4.2 Han

Han et al. (1986) proposed a model for estimating the effect on Vp (2.5) and Vs (2.6) of varying clay content and porosity in brine saturated sandstones. This model is practical as it allows different series of clay content or VShale and porosity to be produced. As this model can estimate Vp and Vs from density and clay content, it is possible to overlay this model in different crossplots including Vp/Vs vs AI.

Hans model for brine saturated sandstones is an empirical model based on laboratory measurement. This means that the equations provided are essentially best fit equations for the rocks in study. It is suggested that empirical models such as these can be difficult to apply to any other rocks other than what was in the original study (Avseth et al 2005). This could make such a model unsuitable for modelling of properties of unrelated rock types. In addition Hans model assumes that Vp is a function of porosity and clay content, where the porosity and clay content are closely related. Other factors such as sorting or cementation, which can affect the porosity, are not incorporated into this model.

$$Vp = 5.59 - 6.93\Phi - 2.18C \tag{2.5}$$

$$Vs = 3.52 - 4.91\Phi - 1.89C \tag{2.6}$$

2.4.3 Constant Cement

The Constant Cement model, Avseth et al. (2000), is a model for sands containing a uniform amount of cement around the grains. The model is constructed for a range of porosities to visualise the change in porosity due geological effects such as sorting. In addition to varying porosity, the fluid content of the model can also be modified using the Gassman equation. The Constant Cement Model can also be added to a Vp/VS vs AI plot to allow a comparison between the model and real data.

The Constant Cement model assumes porosity changes are related to the effects of sorting and that the amount of cement is constant and dependent on depth Avseth et al. (2005). One of the primary variables in this model is the depositional porosity which is related to porosity at time of deposition. Deepwater channel, fan and lobe sands are strongly effected by depositional energy and sorting which means that this model is appropriate for the modelling the sands in this study. The Constant Cement model however, does not take into account any changes in effective pressure or amount of cement. These two variables are likely to change significantly with depth so results obtained for this model are

only valid over a small depth window where cementation occurs and effective pressure is constant.

The model does assume knowledge of the grain and cement properties which can be difficult to estimate without analysis of the physical rock by thin section analysis. In this study the objective is to produce a model for variable porosity to understand how that effects the seismic response. Therefore, it is acceptable to use this model for that purpose with the caveat that the results produced will only show varying porosity for a uniform amount of cement and pressure.

An earlier model, Contact Cement, proposed by Dvorkin and Nur (1996) was also considered for use in this study. In that model the primary variation on the properties of the rock is the amount of cement in the rock. This model would be useful for a comparison between sands at varying depths in a basin where amount of cement can vary significantly. However, as previously mentioned, the goal of this study is to compare models of varying porosity due to deposition rather than cement volume.

$$K_{dry} = \left(\frac{\frac{\Phi}{\Phi_b}}{K_b + \frac{4G_b}{3}} + \frac{\frac{1-\Phi}{\Phi_b}}{K_s + \frac{4G_b}{3}}\right)^{-1} - \frac{4G_b}{3} \tag{2.7}$$

$$G_{dry} = \left(\frac{\frac{\Phi}{\Phi_b}}{G_b + z} + \frac{\frac{1-\Phi}{\Phi_b}}{G_s + z}\right)^{-1} - z \tag{2.8}$$

$$z = \frac{G_b 9K_b + 8G_b}{6K_b + 2G_b} \tag{2.9}$$

K is the bulk modulus

G is the shear modulus

Subscripts "dry" for dry rock, "s" for saturated and "b" for initial.

2.5 Impedance Analysis

Estimation of impedance from well logs can also be used as a indicator of fluid and rock properties. A method proposed by Florez and Kuzmin (2015) relies upon transforming the well data to the impedance domain so that rock properties can be directly related to the seismic response. A key difference is that the impedance domain describes layers of impedance rather than reflectivities between layers as in the case of seismic data. This makes the process closer to the real geology and makes it possible to directly relate rock properties to the impedance contrast.

The method in question relies upon transforming well data (Vp,Vs,Rho) into both

Acoustic Impedance (which equates to impedance at 0 degrees offset i.e. Intercept) and Gradient Impedance which equates to the Gradient.

$$AI = VpRho \tag{2.10}$$

$$lnGI = ln[VpRho^{-4k}Vs^{-8k}] \tag{2.11}$$

K is equal to the average Vp/Vs for the entire data range

2.5.1 Elastic Impedance

Elastic Impedance is a method published by Connolly (1999) and revised by Whitcombe et al. (2000). Elastic Impedance is a modification of the Zoeppritz equation which allows impedance to be modeled at different offsets. Where Acoustic Impedance is the impedance at zero offset, further offsets can be generated using Elastic Impedance which simulate how the impedance response is at any specified offset angle. This process can simulate impedance at angles which match those of seismic angle stacks that have been acquired.

$$EI(\Theta) = \alpha^{ab}\rho^{c} \tag{2.12}$$

$$a = (1 + sin^2) \tag{2.13}$$

$$b = -8Ksin^2\Theta \tag{2.14}$$

$$c = (1 - 4Ksin^2\Theta) \tag{2.15}$$

This results is further stabilised by using the K factor which is an averaging of the data into a background trend (Whitcombe et al. 2000).

$$K = \frac{\frac{^2_n}{\alpha_n^2} + \frac{^2_n+1}{\alpha_n^2+1}}{2} \tag{2.16}$$

Chapter 3

Methodology

This chapter outlines the practical aspects of reservoir characterisation that will be undertaken as part of this study. Firstly, this chapter will discuss how the raw geological well data is interpreted and processed into products that can be used for AVO analysis. This includes calculating interpretation logs, geophysical and elastic properties from the raw well data. This chapter will then discuss the application of different techniques for fluid and lithology prediction including AVO, impedance and forward modelling.

3.1 Data Selection

The aim of this study was to investigate a set of data from the Vøring basin. Selection of Wells to be included in the study was focused around exploration wellbores related to the Astaa Hansten or Luva field and the Asterix discovery which are neighbouring discoveries in the Vøring Basin. Wells from adjacent blocks were also included in the search.

In addition to a geographic selection of wells, the search criteria was also based on available data. In order to apply different AVO modeling techniques on well data a shear velocity or S-Velocity (Vs) log is required. To enable a consistent comparison to be applied the scope of data was limited to Wells with measured shear velocity data available.

The search result yielded 5 wells in total.

1. 6707/10-1 which is the Luva/Astaa Hansteen discovery well from 1997. This well encountered a gas column from 2957m to 3111m.

2. 6705/10-1 was drilled in 2009 on a prospect known as Asterix. This well encountered a 85m column of gas at 3214m coinciding with the Top of the Springar formation.

3. 6605/1-1 was also drilled in 2009 as a down-flank prospect of Asterix known as Obelix. This well also targeted the Springar formation but was dry.

4. 6604/2-1 was drilled in 2011 as target at a class III AVO anomaly believed to be a gas bearing sand. This well was dry.

5. 6704/12-1 was drilled in 1999 and targeted at top Cretaceous formations. This well was returned as a dry well.

The following images shows the location of the five wellbores and discoveries zoomed in as well as their location on the Norwegian Continental shelf as a whole.

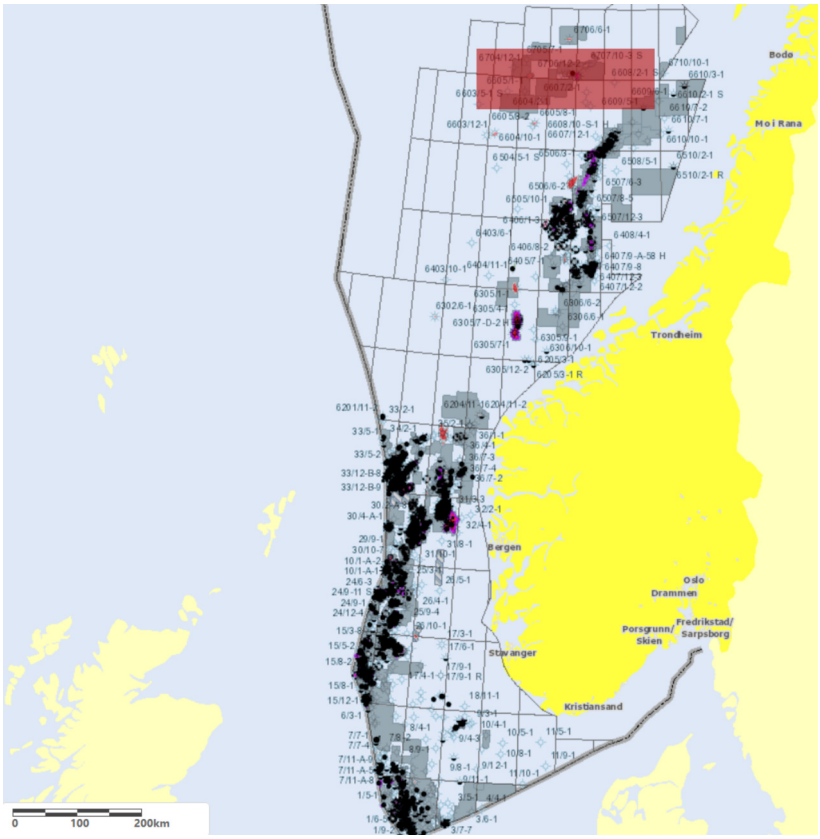

Figure 3.1: Map of Norwegian Continental Shelf excluding Barents Sea

Figure 3.2: Map of the five wells included in the study

3.2 Geological Interpretation

The data set acquired for this study consists of five wellbores complete with wireline logs. Wireline logs or logs are incremental measurements recorded down a wellbore through the geological layers in the subsurface. To analyse the geological properties of the different wells, it is typical to construct a Well Section. This is a 1-dimensional vertical plot with a vertical line representing the depth of each well. Different logs are then added as separate tracks adjacent to the depth line, with different colours and scales for each property. This is an effective way to visualize different properties to make comparisons between wells and for interpretation. Formation information taken during drilling can also be superimposed to help distinguish different zones (Serra 2008). Finally, the logs may be filled with a colour scale to highlight variation in the petrophysical measurements. In order to construct this type of view the data needs to be loaded into an analysis software package. Many types of packages are available for this type of work, but in this case the software tool Petrel was used for the geological interpretation.

The raw data is provided in a standard format known as LAS which makes it possible to standardise many elements of the data including name and property type. This enables the Well Section to have consistent scales, units and properties making it possible to correlate between wells. The logs that are chosen to be added to the tracks in a well section can vary, but for a basic geological interpretation the same standard curves are usually available. In order to classify and understand the geology, a well section was constructed using the following logs:

1. Depth Track (Measured Depth (MD)) - Shows the measured depth of the well in meters

2. Gamma Ray (GR) and Caliper (CALI) - The Gamma Ray log measures natural radioactivity in the rock and essentially contrasts sand, which has a low natural radioactivity, with shale, that has a high radioactivity. The caliper log is also added in this track as a quality control. The caliper runs along the casing of the well and shows where the measurements tools may have encountered problems reading the formation.

3. Density (DEN or RHO) and Neutron Porosity (NEU) - Density and Neutron Porosity are essentially acquired in the same way. Each tool emits an amount of energy from a radioactive source or neutron emitter and measures the absorption from the formation. Density is a measurement of the bulk density of the formation whereas Neutron is a measurement that relates to the porosity of the formation. In order to

make the delineation of sand from shale much more visible these logs can also be setup in a particular way. Density should be reversed and the logs scaled so that in the presence of sand, there should be a significant crossover between the logs. Often this can be colour filled to identify the clean sands.

4. Sonic (DT or DTC) - Sonic measures the velocity or rather the slowness of a formation via the use of a piezoelectric transmitter. This can be useful when combined with the density to estimate acoustic impedance. Sonic is normally expressed in feet per second. Sonic usually refers to compressional velocity or slowness but can also be a measurement of shear velocity, usually called Shear Sonic (DTs)

5. Facies Classification Log - This is an interpreted Facies log using numerical cutoffs of different logs. Neutron and Density are used to distinguish sands from shales whereas sand and gas sand are further distinguished by using the Resistivity.

6. Photoelectric Effect (PEF) - This log measures photoelectric absorption of the formation. This can be a useful log in interpretation of clay and heavy minerals in the formation.

7. Deep Resistivity (RDEP) - Resistivity measures the electrical resistance of the formation. The key objective of this tool is the identification of fluids. Hydrocarbons have a high resistance, whereas brine has a significantly lower resistance.

Figure 3.3 shows a detailed Well section for the 6705 well, highlighting log curves as described in the above section.

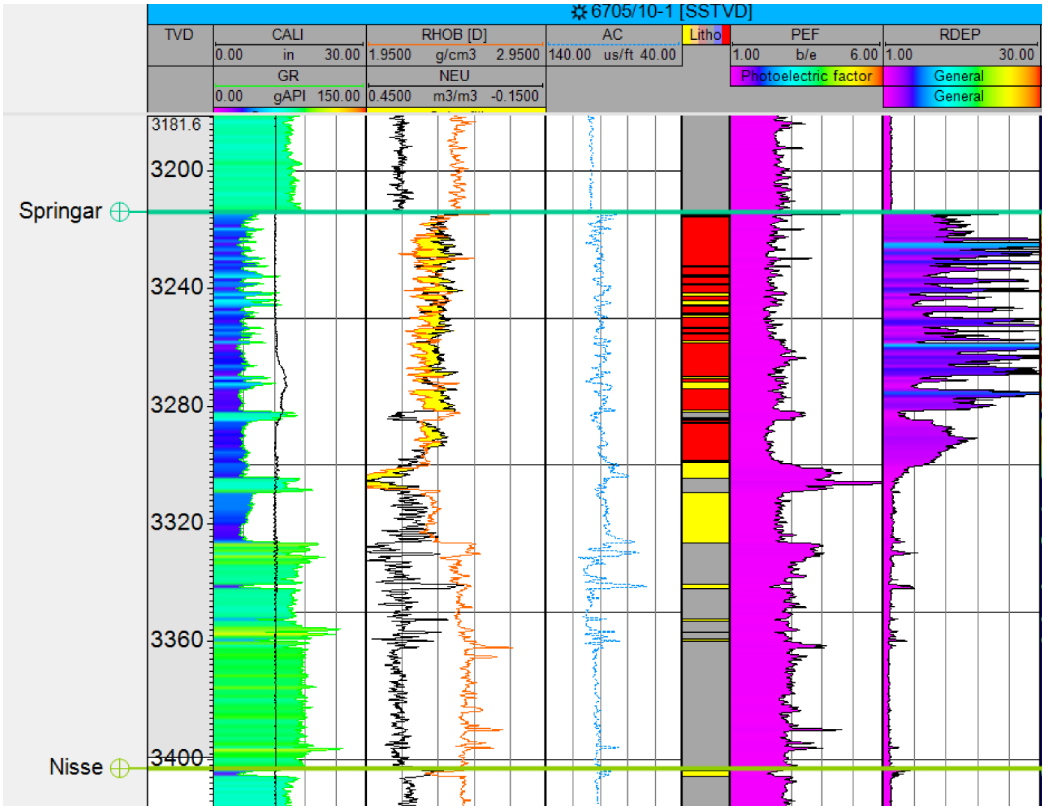

Figure 3.3: 6705 detailed Well section

To summarise the interpretation a short summary known as a reservoir description is usually produced. The following items comprise the key elements of a reservoir description.

- Sand quality and thickness - Estimated from the GammaRay and Neu-Den Crossover
- Sand shale contrast - Interpreted by the comparison of the Gamma Ray between sand and shale and DT or P-Velocity
- Porosity - Estimated from the Neutron log / Neu-Den separation.
- Fluid Content - Estimated from the Resistivity log.

3.2.1 Interpretation Logs

Standard wireline logs are acquired at a well location to measure different properties of the rocks. These measurements, however, do not directly measure physical properties i.e. porosity. Rather they measure something that can be expresses as changes in porosity i.e

Neutron Porosity (Tiab and Djebbar 1996; Serra 2008). To improve the interpretation of these logs from the raw petrophysics the raw logs can be converted into property or interpretation logs. A basic example of this is the conversion of a Gamma Ray log into a shale fraction log. By using the numerical limits of the Gamma Ray log, a shale fraction can be produced through scaling the original values. These physical properties or interpretation logs are required for techniques such as fluid substitution. The following transformations were used to create a set of interpretation logs from the raw logs.

Naturally there a number of assumptions associated with calculating these interpretation logs. For example, the limits of the Gamma Ray used to calculate VShale or the fluid densities used to calculate porosity.

VShale

Percentage of shale in a rock calculated from the Gamma Ray(GR) log.

$$Vshale = \frac{(GR_{log} - GR_{min})}{(GR_{max} - GR_{min})} \tag{3.1}$$

This is calculated for the minimum and maximum of the GR log and the value of the log at a given point.

Porosity

A simple calculation of porosity can be made from density log.

$$\Phi = \frac{Rho_{ma} - Rho_b}{Rho_{ma} - Rho_f} \tag{3.2}$$

Where Rho_{ma} is matrix density, Rho_b is bulk density from the log, and Rho_f is the density of the fluid in place. Effective porosity is also a further expression of porosity which takes into account shale content of a rock. A sand with a higher shale content will have a lower effective porosity than that of a clean sand. Effective porosity is calculated by rearranging the following expression of Porosity.

$$\Phi_t = \Phi_e + VShale \times \Phi_{Shale} \tag{3.3}$$

Water Saturation

$$S_w^n = \frac{R_w}{\Phi^m \times R_t} \tag{3.4}$$

Water Saturation is equal to the resistivity of water divided by the matrix porosity times the measured resistivity.

P Velocity

$$Vp = \frac{10e5}{DTc} * 3.048 \tag{3.5}$$

A simple inverse transformation is used to calculate the P-Velocity(Vp) from the compressional Sonic(DTc), which measures slowness of the rock in f/s

S Velocity

$$Vs = \frac{10e5}{DTs} * 3.048 \tag{3.6}$$

Similarly S-Velocity(Vs) is calculated from the shear Sonic(DTs).

3.2.2 Interpretation Section

As outlined in the previous section, after processing of the raw data into physical properties, a new well section was created using the calculated logs. This well section includes the following logs:

1. Depth Track - Shows the depth in meters
2. Water Saturation (Sw)- Fraction of Water vs Gas Saturation
3. Effective Porosity (Peff)- Measure of the absolute porosity
4. Shale Volume (Vsh)- Percent Fraction of the shale in the rock
5. Neutron and Density (NEU and RHO) - Same as geological well section, but useful lithology indicator
6. Interpreted Lithology - Interpretation of Facies based on NEU-RHO and RDEP

A section showing the calculated logs can be found in Appendix A

3.2.3 Core Images

Physical core taken from Well 6707 was also available as digital photos together with the log files. These images are used in Chapter 4 which describes the geology of the study area.

3.2.4 Geological Cross Plots

In addition to a Well Section, petrophysical logs can also be analysed in a cross plot to aid interpretation. For this type of analysis it was decided to migrate the data to Matlab in order to allow for a more in-depth statistical analysis of the data. The data sets for each well were re-sampled to the same depth increment and then exported as a .csv file for loading into Matlab.

The most common and useful plot for geological interpretation is to plot Neutron against Density (Tiab and Djebbar 1996). Neutron is plotted on the X-Axis and density on the Y-Axis which is reversed, as per the convention for Neu-Den interpretation (Tiab and Djebbar 1996; Serra 2008). This is to mimic the same situation of the well section, where the neutron and density crossover highlights clean sands. This cross plot is an effective way of visualising data as the different lithologies tend to separate out into clusters. Gradual changes in lithology can however hinder the use of this type of plot. Naturally, both the well section and cross plot techniques were combined to make a thorough interpretation of the geological data.

3.2.5 Elastic Properties Analysis

The elastic properties of the rocks (Vp,Vs,Rho) can also be analysed in a similar manner using cross plots. Typically this is done by converting Vp and Vs into a ratio of Vp/Vs (Avseth and Ødegaard 2004) and plotting against acoustic impedance(AI). This plot essentially encompasses the three elastic components of a seismic reflection.

A cross plot of VP/VS against AI can be a useful fluid and lithology indicator(Chi and Han 2009; Gupta et al. 2012). This is due to the influence that fluids have on the compressional velocity (Vp). Replacing brine, which is compressible with gas which is not, decreases Vp. Since Vs is unaffected by fluid, the Vp/Vs ratio will be significantly lower for gas than for brine. Using Vp alone would prove inconclusive as lithological changes can also influence the Vp.

This approach, favored by many authors including Avseth and Ødegaard (2004) and Chi and Han (2009), is useful for interpretation and also allows the integration with theoretical rock physics models. However, from this plot, it is not possible to directly relate trends in the plot to changes in the seismic reflections(Florez and Kuzmin 2015).

3.3 AVO Analysis

Prior to AVO modelling, the data was processed by applying a depth filter to divide each well into sets of overburden and reservoir. The reservoir zones have been identified from the original well report and are shown in Appendix A. The zones of overburden and reservoir were then averaged into a single value of Vp,Vs and Rho. Reflectivity could then be calculated using the Aki Richards equation (2.2.1) with the mean Vp,Vs and Rho. The reflectivity was also calculated at each offset angle between 0 and 30 degrees. Results can then be analysed in a plot of Reflectivity vs Offset. It should be noted however that this calculation differs from the Shuey equation which is used to directly estimate Intercept and Gradient.

3.3.1 AVO Class Plot

Using the Shuey equation, Intercept and Gradient can be directly calculated from the values of overburden and reservoir for each well. This can be plotted on a Intercept vs Gradient cross plot. This plot is centred around 0 which allows for both positive and negative values. In addition, a set of guidelines can be added to split up the plot into classes from the traditional AVO classification scheme. A line of Intercept equal to Gradient is also added to provide an estimation of a background trend. This approach follows the method outlined by Castagna et al. (1998).

3.3.2 Stochastic Modelling of Reflectivities

The average method, outlined in the previous section, results in only a single point for each well when plotted on an Intercept vs Gradient cross plot. Avseth et al. (2005) suggest that this can be improved by the introduction of Monte Carlo or stochastic modelling steps. Since averaging of the data many not be fully representative of the overall variation of the data, this will be improved through a stochastic approach.

Random Numbers can be generated from a set of related variables which have a multivariate normal distribution (Thomopoulos 2013). Multivariate random number generation can be used to simulate a new set of numbers based on two or more dependent variables.

This technique is valid in this scenario as Vp,Vs and Rho are dependent variables which constitute a seismic reflection. The algorithm used in this case returns a matrix of random values calculated from a mean Vp,Vs and Density and Covariance Matrix for a particular overburden and reservoir facies.

The parameters or description of the data required to generate random samples using this technique are, a mean value - MU and a covariance value - Sigma. Mu in this case will be a data set consisting of the mean of each of the variables, in this case Vp,Vs and Rho. Sigma will be a covariance matrix of each of the variables in a data-set.

Covariance Matrix

Central to the calculation of random variables is a statistical summary of each data set known as a covariance matrix. A covariance matrix describes how each of the pairs of variables moves with respect to one another and hence is a good description of a set related variables. An example covariance matrix is given below. It consists of a measure of variance of the individual variables plus a measure of covariance between each pair. The covariance matrix shows the covariance between variables and the individual variance along the main diagonal (Thomopoulos 2013)

Table 3.1: Covariance Matrix

	Vp	Vs	Rho
Vp	Var(x1)	Covariance(x1,x2)	Covariance(x1,x3)
Vs	Covariance(x1,x2)	Var(x2)	Covariance(x2,x3)
Rho	Covariance(x1,x3)	Covariance(x2,x3)	Var(x3)

3.4 Forward Modelling

Forward modelling techniques can be used to estimate how different fluid and lithological conditions effect the elastic properties of the rock. This can be used to compare different scenarios with the original data. This provides a means to link AVO to certain changes in fluid and lithology. The following section outlines how the different forward modelling techniques were applied in this study.

3.4.1 Fluid Modelling

By applying the Gassman equation an estimate can be made on the effect of chaining the fluid in the reservoirs. In the present study, this has been run individually on each of the five wells to create new data from which a reflectivity, intercept and gradient can be estimated. The following inputs are required for the Gassman fluid substitution process:-

1. The original elastic properties (Vp,Vs,Rho)

2. Shale fraction (Vshale) - Used to calculate original bulk and shear modulus from the Hill Average mixing method and mineral properties.

3. Effective Porosity (PHIE) - Used to specify the pore space occupied by fluids.

4. Water Saturation (Sw) - Used to define the original fluid in place

5. Fluid Properties - Bulk and shear modulus and density of original and new fluids

6. Mineral Properties - Bulk and shear modulus and density of minerals.

The three dry wells were simulated brine to gas and the two gas well from gas to brine. The fluid and mineral properties used to do this are listed below. The mineral and fluid properties are standard values used by many authors in North Sea fields with a normal pressure regime. These values are originally from Wang et al. (2001) and Carmichael (1999).

Table 3.2: Fluid properties brine to gas

	Fluid Initial	Fluid Final
Bulk Modulus	2.75 GPa	0.1 GPa
Density	1.025 g/cm3	0.23g/cm3

Table 3.3: Fluid properties gas to brine

	Fluid Initial	Fluid Final
Bulk Modulus	0.01 GPa	2.75 GPa
Density	0.23 g/cm3	1.025 g/cm3

Table 3.4: Mineral Properties

Mineral	Bulk Modulus	Shear Modulus	Density
Quartz	37 GPa	44 GPa	2.65 g/cm3
Clay	30 GPa	10 GPa	2.6 g/cm3

Once run, the equation produces a new set of Vp,Vs and Rho logs as well as a Kmin and Kdry which is used for quality control. The new sets of Vp,Vs and Rho are then averaged in the same way as the raw data and used to estimate new reflectivities.

3.4.2 Porosity Modelling

By using the Constant Cement model described in the section 2.4.3, a model of Vp, Vs and Rho can be calculated for different porosities and fluid saturations. Using this model,

the effect porosity and fluid has on Vp,Vs and Rho can be quantified. A model was produced using values of 40% for depositional porosity and same values for minerals and fluid properties mentioned in the previous section. Two series of data from this model, 100% Brine and 100% Gas with varying porosity were plotted against the original data in a Vp/Vs vs AI cross plot. The elastic values for increments of 5% porosity between 10% and 30% were then used to calculate a reflectivity, AVO and synthetic for each porosity value.

3.5 Impedance Modelling

3.5.1 Gradient Impedance

This method relies upon transforming well data (Vp,Vs,Rho) into both Acoustic Impedance and Gradient Impedance which equate to the Intercept and Gradient of the reflectivity domain. These properties were then analysed in a cross plot of AI vs GI. Plots were then annotated using a third colour axis for both VShale and Sw. This allows the plots to link lithological and fluid changes to changes in AI and GI.

3.5.2 Elastic Impedance

Calculating elastic impedance (EI) for each well was done using the equations specified in section 2.5. A calculation was done at three offsets, 0, 15 and 30 degrees. This roughly approximates to the Near, Mid and Far angles that are typically delivered with seismic data sets.

Producing data at these angles allows a direct estimation of what geological features in the seismic will contrast at this angle. This must be correlated together with raw logs to identify which property is contrasting i.e. fluid or lithology.

Acoustic impedance is also added as a quality control, as it equates to an EI at 0 degrees of offset.

3.6 Methodology Summary

In summary, the main goal of the project is to run various modeling techniques on the well data from the Vøring Basin to compare the results. After a preliminary interpretation and processing the data will be modeled using various methods to change fluid properties, modify porosity or calculate AVO. The results of which will be compared and contrasted in various results plots like the AVO Classification, VpVs against AI plots. The study also

aims to contrast various forward modelling techniques with the impedance work-flow which has its own method and set of results plots.

A summary diagram of the methodology is given below

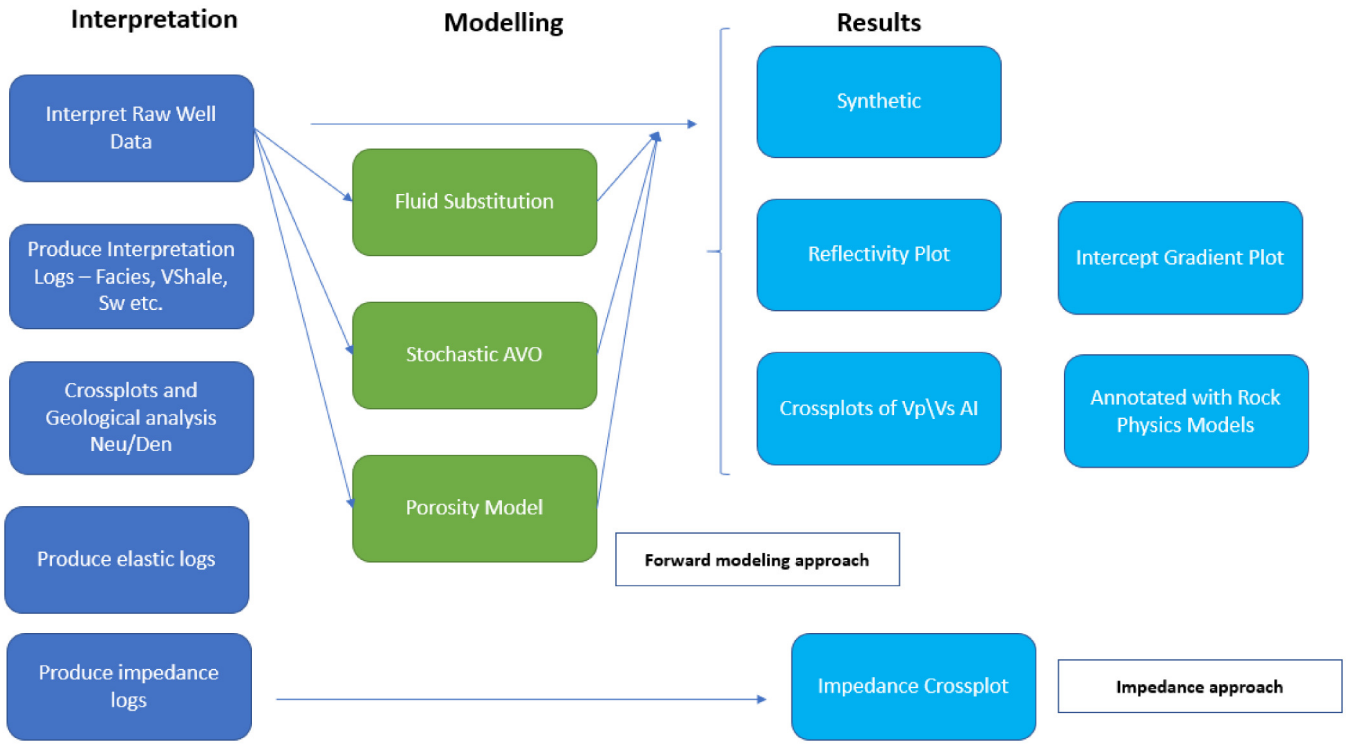

Figure 3.4: A schematic summary of the methodology of the study

Chapter 4

Geology, Tectonics and Stratigraphy of the Study Area

This chapter outlines the overall geological setting for the data in the research project. Putting this type of analysis in the correct geological context is an important step in ensuring that the observations in the data can be tied back to a real-world setting. This chapter also gives a brief introduction to the geology and tectonics of the study area. These act as important controls on the deposition of sediments which controls the distribution and quality of any potential reservoirs.

4.1 Study Area

All the Wells in the Study area reside in a geographical location known as the Vøring Basin. The Vøring Basin is located between 70 to 78 degrees N and 3 to 10 degrees E. It is roughly located offshore Mid Norway in the Norwegian Sea area. Figure 4.1 shows an approximate location of the Vøring Basin in relation to present-day Norway and the Paleo-Reconstruction location of East Greenland.

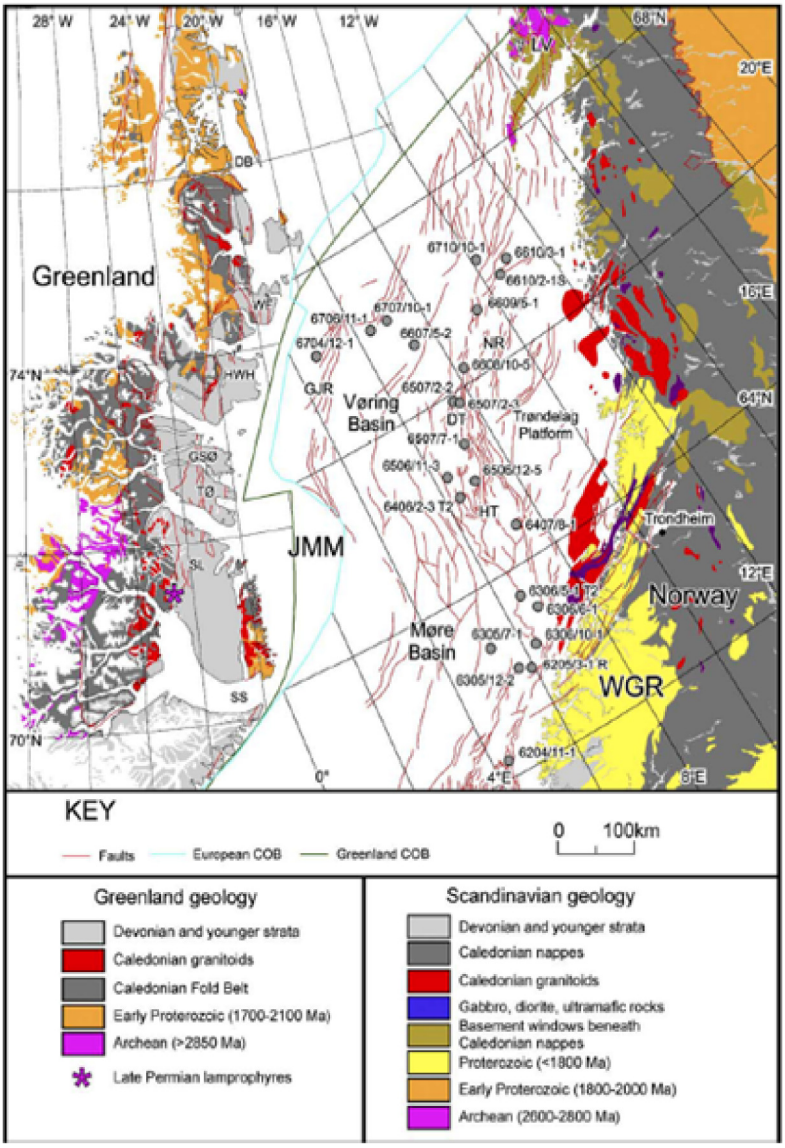

Figure 4.1: Pre-Rift map of the Vøring Basin from Knaust (2009)

4.2 Tectonic Development

The Norwegian Continental Shelf is a passive margin that has undergone many phases of rifting until its present day formation of the Norwegian Sea Basin. The Vøring Basin area started to develop during a period of rifting which started in the Mid to Late Jurassic in the area currently between Norway and East Greenland. This resulted in the formation of

a failed rift between Norway and Greenland (Shanmugam et al. 1994).

Following this period of rifting a period of thermal subsidence occurred which caused a deepening of the basin and caused a deep marine environment to develop during the Cretaceous and Palaeocene (Knaust 2009). A further period of rifting occurred throughout the Late Cretaceous eventually leading to the separation of Norway and Greenland and the opening of the North Atlantic (Laurent et al. 2012)

Structurally, the Vøring Basin is flanked by the Trondelag Platform to the South East and the Gjallar Ridge to the North West. Between the main structures a number of NE-SW synclines and anticlines have been formed as a result of the overall tectonic stress during the Late Cretaceous (Laurent et al. 2012). These elements were the main controls on sediment deposition during that time. Figure 4.1 illustrates the main structural elements of the Vøring Basin, the bounding Gjillard Ridge (GJR) and Trondeleg Platform and shows the main NE–SW trending structures.

Fjellanger et al. (2005) suggest that during rifting in the Late Cretaceous, structures in the Vøring Basin lead to the development of large basin-floor fan systems. Local faults and transfer zones were the main control on the distribution of sediment. It is suggested that the depositional systems were quite large and formed many laterally extensive reservoirs (Fjellanger et al 2005; Knaust 2009). The source of the sediment for these deep marine fans was likely from the East Greenland Shelf towards the South West (Knaust 2009). Sandstones of this age in the Vøring basin are almost exclusively related to deep water slope and submarine fan type environments (Morton et al. 2004). The following figure 4.2 shows a schematic diagram of the geological environment during the Late Cretaceous in the Vøring Basin. A further period of rifting is then thought to have affected the Vøring Basin in the Late Cretaceous and Early Tertiary. Morten et al. (2014) suggest that this led to further subsidence and burial of the sediments.

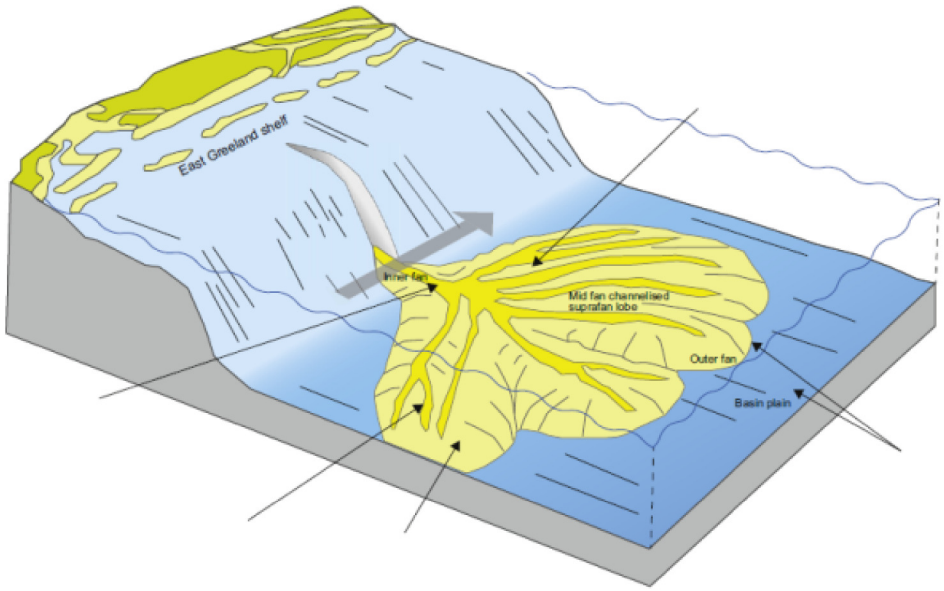

Figure 4.2: Geological model for the Vøring basin in the Late Cretaceous from Knaust (2009)

4.3 Stratigraphic Units

The Upper Cretaceous units found in all wells in the study area contain four formations of the Shetland Group. These groups consist of the Upper Santonian - Kvitnos Formation which consists of claystones, the Nise formation of claystones with sandstone interbeds and finally, the Springar formation of mudstones and interbeddded carbonates and sandstones (Gardstein et al. 2010). The Kvitnos formation is considered post rift in the Jurassic to Cretaceous, Nise between the two phases of rifting and the Springar in the synrift of the Late Cretaceous (Setoyama et al. 2013). Figure 4.3 illustrates the Stratigraphic column for the basin. The oil and gas reservoirs in the areas can occur in Nise and Springar formations often, overlain by shales and mudstones of the Top Springar or Tang formation.

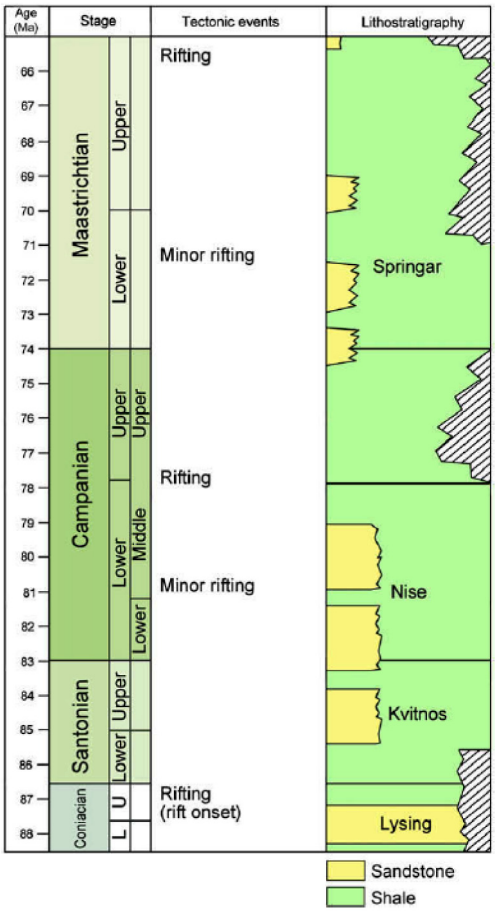

Figure 4.3: Stratigraphic Column for the Vøring Basin from Knaust (2009)

The focus of this study is essentially the relationship between the background shales and mudstones of the Springar and Tang formations, to that of the sands in the Springar and Nise. The boundary between shale and sand is an important acoustic contrast in the seismic data which often leads to a strong AVO response.

4.4 Reservoir Description

Although linked to different chronological events the sands of the Springar and Nise formation are very similar in nature and are considered to be deposited by identical processes. Core images from the 6707/10-1 Well give a good insight to the nature of each of the facies. This is discussed in the following section.

4.4.1 Shales, Mud Stones and Claystones

These are largely deposited as pelagic layers in a deep marine environment by sediments carried deep into the basin. These are typically laminated deposits of very fine material from pelagic fallout (Godall et al. 2002). The section also shows frequent interbeds of coarser sand and silt material deposited by low density currents. Figure 4.4 shows a section of Shale from the 6707/10-1 Well.

Figure 4.4: Shale section from the 6707/10-1 Well

This images shows the thicker sections of dark laminated fine materials from pelagic fallout, interbedded with lighter coloured silts and fine sand.

4.4.2 Sand

The sands in the basin are typically form higher energy deep marine channels and turbidity flows. These are typically channel and sheet sands which form part of large channel, lobe and fan bodies in the basin (Knaust 2009; Goodall et al. 2002). The thickness of the sand bodies is therefore highly variable, from large thick sheet and channel sands to thin channels and lobes. Sand bodies are also often separated by layers of shale (Goodall et al. 2002). Figure 4.5 shows a thick sand sequence from the 6706/10-1.

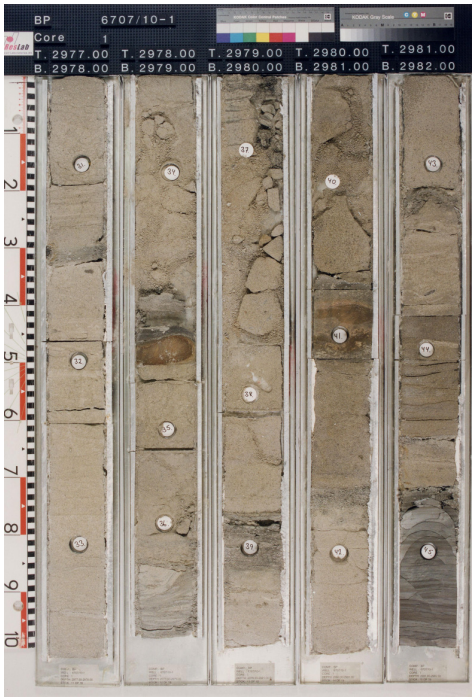

Figure 4.5: Sheet sand of the Nise Formation 6707/10-1 Well

4.4.3 Shaley Sands

In this depositional environment, there is also a setting between the high energy channel setting and the background pelagic environment. Such units are comprised of mostly shale and silt with sand interbeds. These units are often laminated in appearance. The sand in the thin interbeds can be high in quality but in very fine beds. Godall et al. (2002) suggest that these deposits are likely deposited at a distance away form the main channels and fans. Figure 4.6 illustrates a typical sand to shaley sand sequence. Thin parallel lamination can be clearly seen on the lower part of the section.

Figure 4.6: Shaley Sand facies 6707/10-1 Well

Chapter 5

Results

This chapter details the observed results based on the methodology and techniques discussed in Chapter 2: Theory and Chapter 3: Methodology. Firstly, this chapter summarises the interpretation of the raw well data, which gives an understanding of the different target reservoirs and their reservoir quality. After a preliminary interpretation, the results of analysing the data through various cross plots is then discussed. This is followed by a section on fluid substitution of the raw well data.

Next, an analysis of the reflectivity and AVO effect of the different reservoirs is presented, followed by a reflectivity and AVO estimate for the different fluid scenarios. This is presented in this way to group together the AVO elements of the process.

Afterward, the results of analysing the data against several different rock physics models are presented. Results from the rock physics modelling is used to produce a matrix of simple synthetic models of varying porosity and fluid.

Finally, this chapter is concluded by showing the results of the fluid and lithology prediction workflow in the impedance domain. This has a similar approach to the previous workflows using a combination of cross plots and modelling steps to produce results.

5.1 Interpretation Results

5.1.1 Geological Results

Figure 5.1 shows a correlated Well Section display for the Lower Cretaceous formations of the wells in the study area. For each well the available data is divided into tracks. The Well Section has also been flattened on the Springer Formation which is one of the key markers in the area.

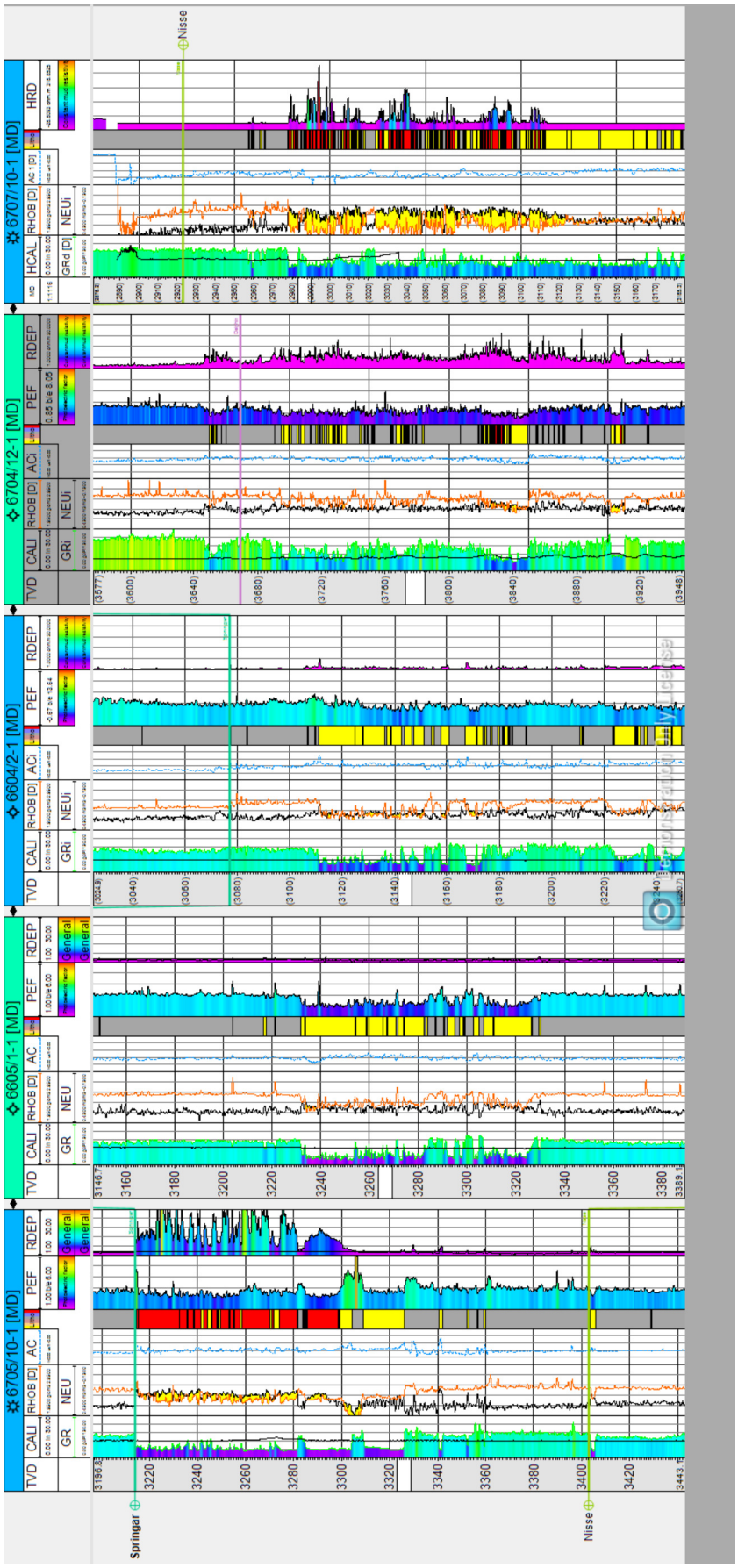

Figure 5.1: Cross Sections of the Well Data showing Petrophysical Logs and Lithological Interpretation

The Well Section of the raw logs shows the five wells and highlights the main geological aspects of the study data. The Gamma Ray Log shows the main contrasts between sand and shale. The deep purple colours indicate low Gamma Ray which should indicate clean sands. This can be correlated with the separation of Neutron and Density (Neu-Den) which also identifies clean sands, indicated by the yellow colour fill. The crossover between neutron and density can be a useful indicator for very high quality sands that are desirable exploration targets.

In addition, the resistivity curve can show the presence of hydrocarbons in the well. In the case of well 6707 we see a large increase in resistivity due to the effect of gas in the sandstone unit. 6705 also shows this trend. The other two wells, 6604 and 6005, show no spike in the resistivity which suggest they are brine saturated. Well 6704, although classed as dry does show some response on the resistivity.

Finally, a coloured facies log shows the main facies based on combining the sand-shale contrast from the Neu-Den and fluid from resistivity. This shows sand in yellow, gas sand in red and shale in grey.

A short reservoir description of each reservoir section is summarised in table 5.1.1.

Using a scatter plot or cross plot of Neutron vs Density it is then possible to visualise the reservoir zones in more detail. Figure 5.2 shows a Neutron-Density cross plot for each of the wells. Note that the convention for this type of plot requires destiny to be decreasing up the Y-Axis. The Neutron-Density cross plots are configured in the same way as the neutron and density tracks in the Well Section i.e. the same scale and the density axis is reversed. This is done to highlight separation and crossover. In this plot the colour of the points is generated from the calculated VShale log to help add some context. On this plot, "crossover" occurs when points move towards the upper left quadrant of the cross plot.

The two wells with gas saturated reservoirs 6705 and 6607 show a clear crossover and separation between sand (yellow) and shale points (greens and blues). This plot shows that although 6707 is slightly shalier than 6705, it has a stronger crossover. Well 6604 shows a unique scenario where the shale points plot to the lower left quadrant rather than the lower right, which is the case with all the other wells. This could indicate a different type of shale or a very shaley sand.

The other two wells show less of a separation between sand and shale and more clustered data points. This section appears to represent a shaley sand, which is a mixture of sand and shale rather than one or the other. Well 6704 is also significantly deeper than the other wells which may imply a lower porosity and result in the observed trend towards the lower left.

This plot is an effective technique for understanding where the good sands will plot

Table 5.1: Well Description

Well Name	Sand Quality and Thickness	Sand Shale Contrast	Porosity	Fluid Content
6604/10-1	Highly variable quality and thin reservoir	Moderate contrast between sand and shale decreasing with depth	The porosity is moderate	Brine
6605/1-1	Moderate to clean thick sand with shaley intervals	Moderate contrast between sand and shale, low AI contrast	The porosity is moderate but variable	Brine
6704/10-1	Good quality but thin	Good separation but appears gradational	Good porosity	Brine or low saturation of gas
6705/10-1	Thick sequence of clean sand	Strong separation between sand and shale	Good and constant	Gas saturated
6707/10-1	Good quality thick sand with shale intervals	Good contrast and strong separation	Good porosity	Gas saturated

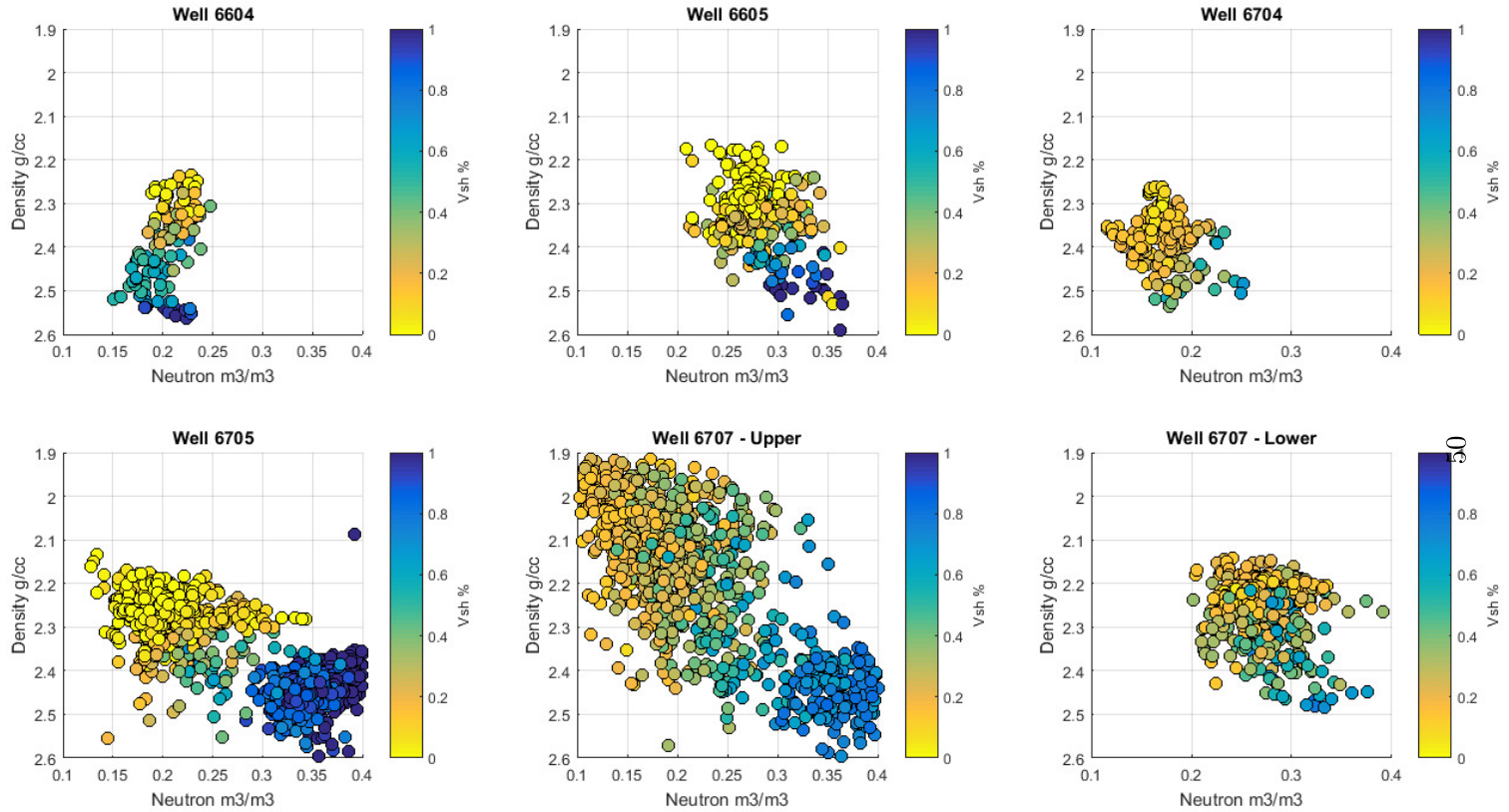

Figure 5.2: Crossplot for Neutron Density

and a good indicator of which of the reservoirs are favourable. However, this plot does not offer much information to help with the seismic mapping of reservoir facies.

5.1.2 Geophysical Cross plots

Vp/Vs vs AI

Figure 5.3 shows the results of creating a Vp/Vs against AI cross plot. This figure shows that this type of cross plot is useful for separating out different facies and fluids. The gas saturated sands show a clear separation as they have a distinct low Vp/Vs ratio (Vp/Vs $>$ 1.6). This is clearest on the 6707 well as it is split into an upper and lower section. The upper section shows a gas sand with a shale overburden whereas the 6707 Lower plot shows primarily a brine sand. The 6705 well also shows this low Vp/Vs ratio, but rather exhibits a single large cluster of points which perhaps implies a more gradational change. Well 6605 shows some similar trends towards the lower Vp/Vs values. This well is classed as dry and has a flat resistivity. The points in this well may be very good clean high porosity sands, but lack any hydrocarbon saturation which would move them further down.

Well 6604 shows a tightly clustered set of sands and shale points with a higher Vp/Vs ratio. This indicates that well 6604 is a poor potential reservoir with a higher shale content that those of 6705 and 6605.

Finally, the 6704 well shows a unique clustering towards the lower right quadrant. Due to the increased depth, this zone may be more compacted and have a lower porosity leading to this trend towards the right. This well may also have a small saturation of hydrocarbons which contribute to the lower Vp/Vs ratio.

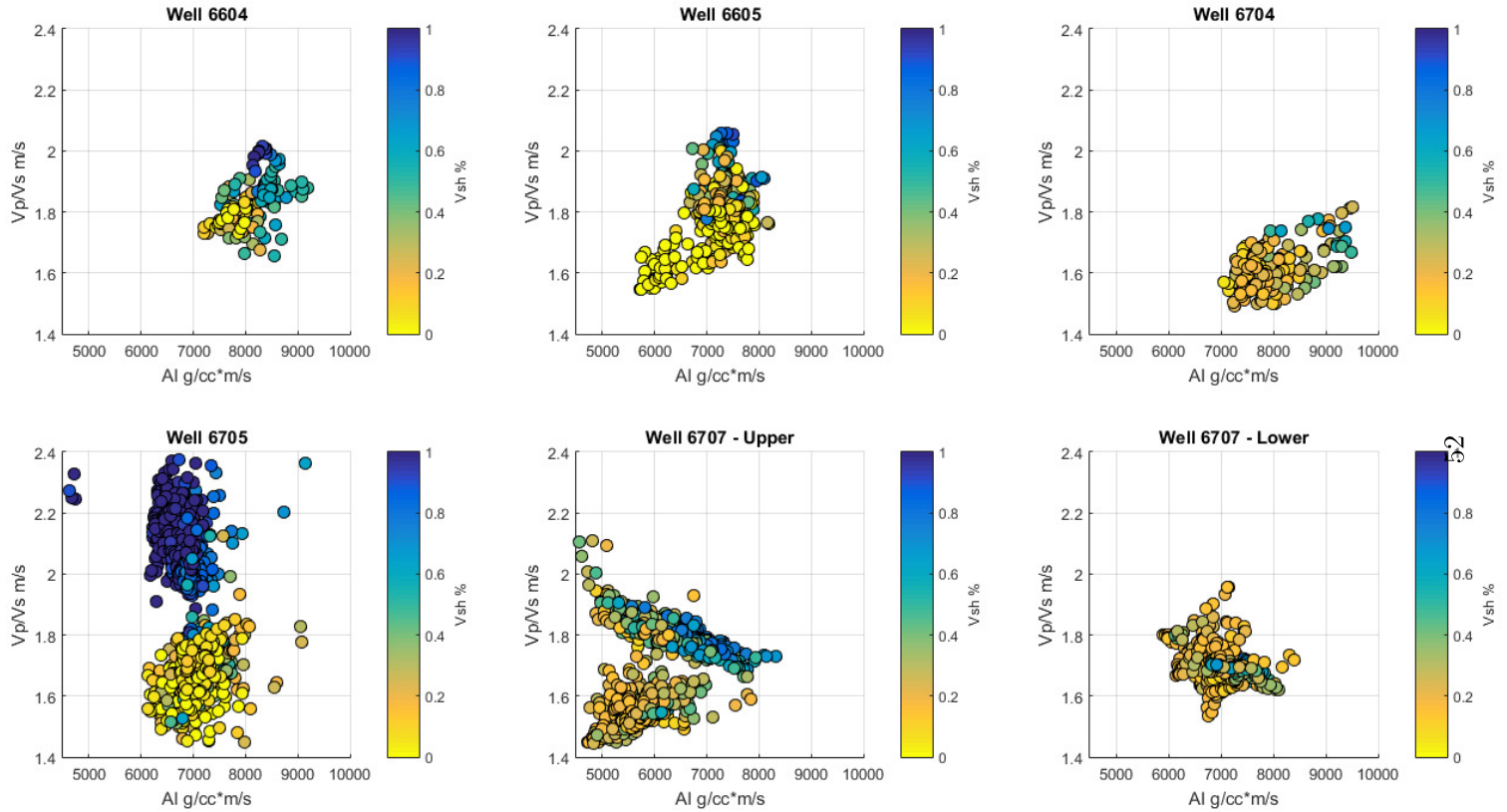

Figure 5.3: VpVs vs Acoustic Impedance Crossplot

5.2 Fluid Substitution Results

The following section details the results from the application of fluid substitution on the input data. The fluid substitution was applied on all the main reservoir sand data points i.e. it was not applied on the shale points, hence why there are fewer points displayed in the results. In addition, following the fluid substitution the reflectivities have been recalculated, this is discussed in section 5.3.3 together with the other AVO results.

This first stage of the Gassman process is to simulate the rock to dry, Figure 5.4 shows a plot of Porosity vs Normalised Bulk Modulus. This plot describes the stiffness of the rocks and implies how the bulk modulus will be effected by changes in fluid.

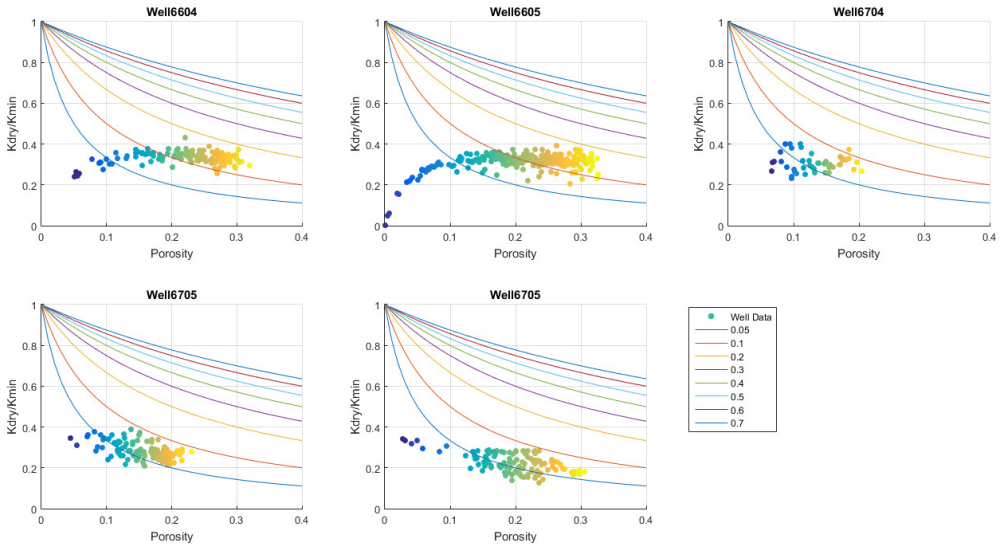

Figure 5.4: Rock stiffness or Normalised bulk modulus plot

Figure 5.4 shows that although there is some minor variation in the stiffness, all the reservoirs should respond similarly to the substitution of fluid. Well 6704, due to the higher depth, would be expected to be the stiffest rock and lowest porosity rock. This agrees with what is observed in the stiffness plot. Well 6704 mostly plots to the lower left, whereas the other wells have higher porosities and plot more towards the right. The flat trend of the data suggests that the response to changes in fluids would mostly be influenced by the porosity of the rock.

Figure 5.5 shows a cross plot matrix of the different results from fluid substitution. The results for well 6605 and well 6604 show a typical result where there is a clear separation

between brine or gas saturated points. Well 6605 in particular shows that gas saturation results in a trend towards the lower left of this plot. As expected well 6704, is stiffer and shows less movement as a result of fluid substitution.

Well 6705 shows the same trend to the lower left and nearly all gas points are thrown up to the upper right when brine is substituted in place of gas. However, it still results in a large cluster and overlap with the original points. The average or centre point of these clusters should result in two distinct values for Vp,Vs and Rho, despite the plot appearing to have significant overlap.

Well 6707 shows a slight trend towards the upper right with substitution of gas to brine, but the result looks less clear than the other wells due to the large overlap. The reservoir of the 6707 well consists of a thick sand unit with frequency shale interbeds. These shale interbeds in addition to the sands are the reason for the bimodal distribution of points for the 6707 well.

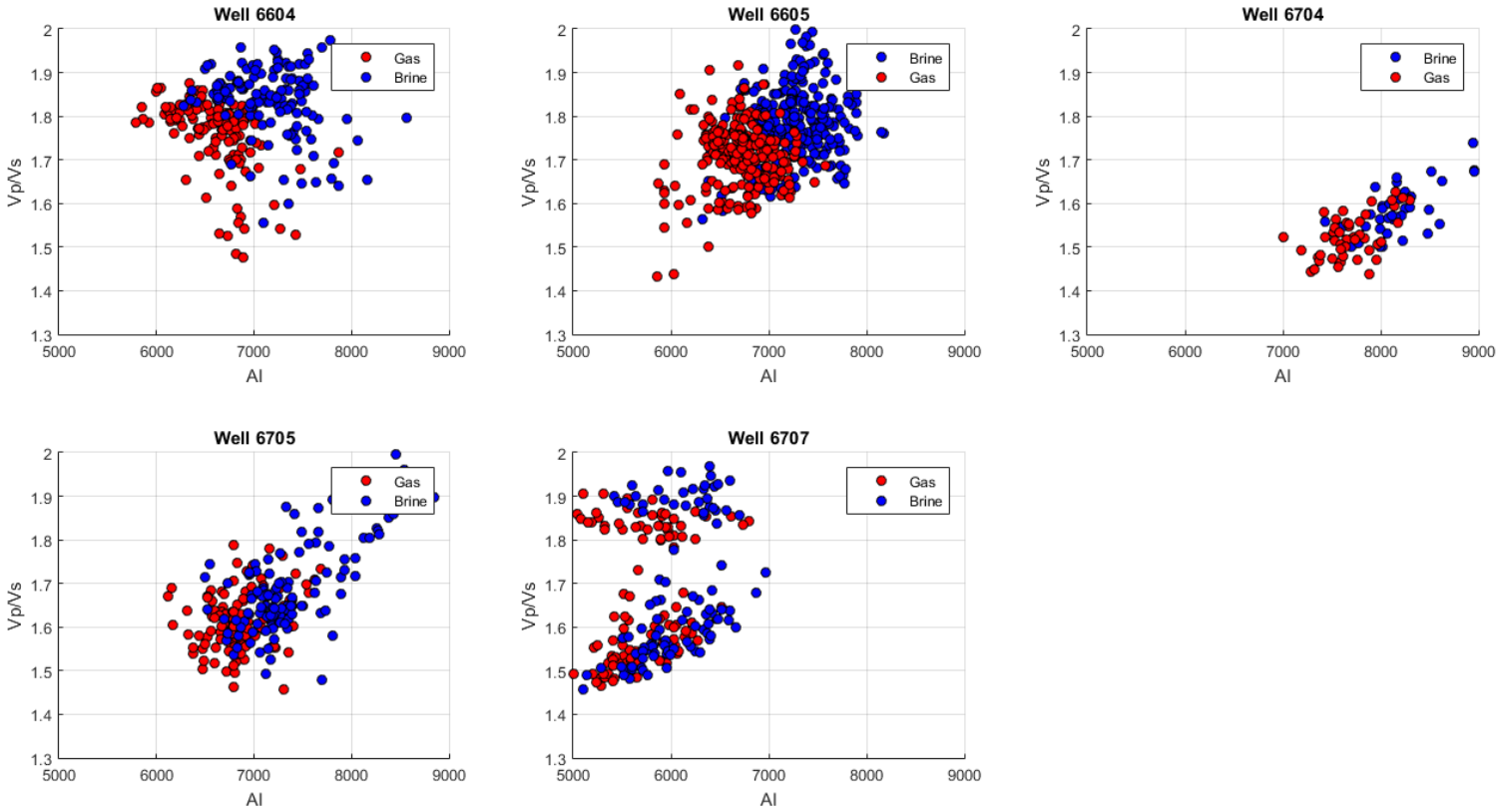

Figure 5.5: Fluid Substitution all wells

5.3 Reflectivity and Synthetics

Figure 5.6 shows the reflectivity calculation result with offset for each of the five reservoir zones. What is noticeable from this plot is that wells 6604 and 6605 have very similar responses. Both have a small negative intercept and small negative gradient. Well 6705 has a significantly higher gradient than all other reflections but a small intercept. Well 6707 has a large negative intercept and negative gradient. This is typical of a gas response.

Well 6704 has however, a somewhat different result that the others. It has a much higher intercept, meaning acoustic impedance contrast, but flat or positive gradient. In this case 6704 shows as a Class IV which is characterized by a large negative intercept and positive gradient. Positive gradients are associated with a decrease in S-Velocity across the boundary (Simm and Bacon 2014).

Analysis of the logs shows that the Vs for 6704 is relatively flat at this depth compared with 6705 which shows a large increase across the boundary between the overburden and gas sand. A figure showing the geophysical logs can be found in Appendix A.

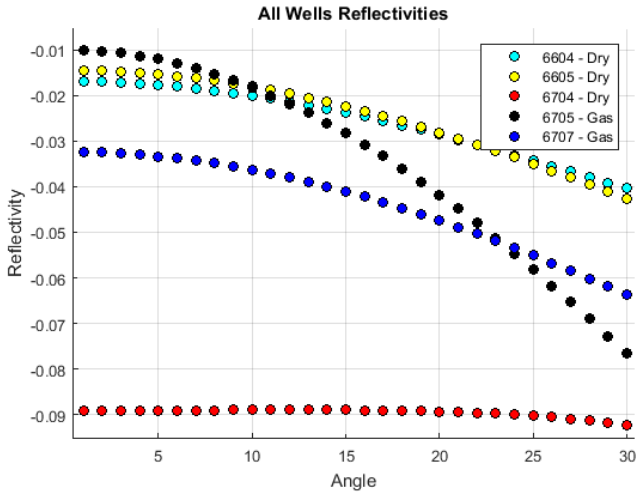

Figure 5.6: Plot of each wells reflectivity between overburden and reservoir zone

Figure 5.7 presents a simple blocked model for each well for overburden, reservoir and underburden. This plot shows a simple synthetic for each of the reservoir in the area. This is based on the reflectivity calculation using the Aki-Richards equation.

All boundaries between overburden and reservoir result in a negative amplitude, meaning that the reservoir has a lower impedance than that shale overburden. Well 6705 shows a typical example of an amplitude variation with offset. The overburden to reservoir boundary shows a clear negative response at low offsets which becomes more negative with

offset. The next reflection is the gas-water contact, which is also changing with offset, this time becoming more positive as the brine sand has a higher impedance than the gas sand. The final reflection on this plot is that of the brine sand and shale underburden. This is another positive amplitude as the shale has a higher impedance, but shows less of an AVO effect than the other two reflections.

These results demonstrate that building a set of reflections in this way, can be an important way of understanding the expected AVO behaviour of the different boundaries in the seismic data.

Some elements, however, disagree with the result when calculating the Intercept and Gradient directly by using the Shuey Equation (detailed section 5.3.1). For example, well 6604 does not show a positive gradient. Rather it shows as slightly negative or even neutral. Well 6707 also does not show a large AVO effect, but it may be so large that it is being clipped by the colour bar, which was set to enable a comparison between the five wells.

5.3.1 AVO

Figure 5.8 is an AVO plot which summaries the Intercept against Gradient response of the five wells. This calculation is done using the Shuey equation (2.2.3). This plot more or less confirms what is observed in the reflectivity, with a few exceptions that were discussed in the previous section.

Here the plot is divided up into classes and has a background trend which represents a 1:1 ratio between Intercept and Gradient. It can also be see that the two gas discoveries plot far away from the background trend. However, in the case of well 6707 it would be classified as a Class II similar to 6604 and 6605.

It can be seen from this example, that in order to use the scheme to detect the presence of gas, it would seem logical that the response must have either a large Gradient or large Intercept with moderate gradient. It's not enough as in the case of well 6604 and well 6605 to have a moderately negative intercept and gradient.

Well 6704 has a unique response. The well 6704 is at a significantly larger depth than the other reservoirs which may influence the porosity through higher cementation or compaction. The VpVS AI plot (figure 5.3) shows that the sand and shale of this well has slightly different properties compared with the rest, for example the reservoir and overburden have a higher AI than all of the other reservoirs.

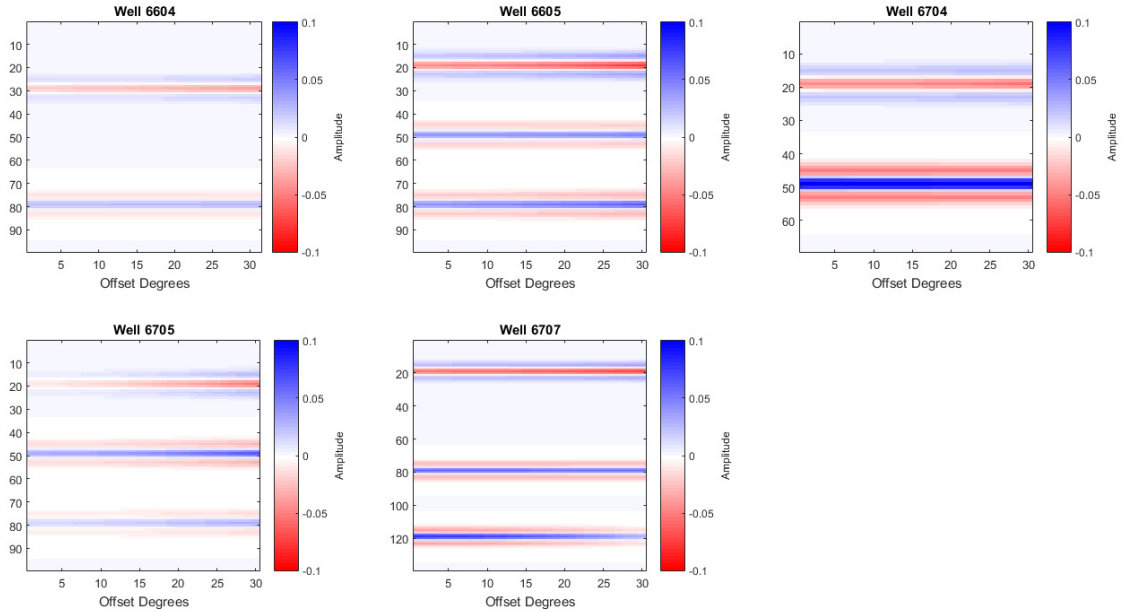

Figure 5.7: A blocked model Synthetic for each reservoir zone with varying angles of offset

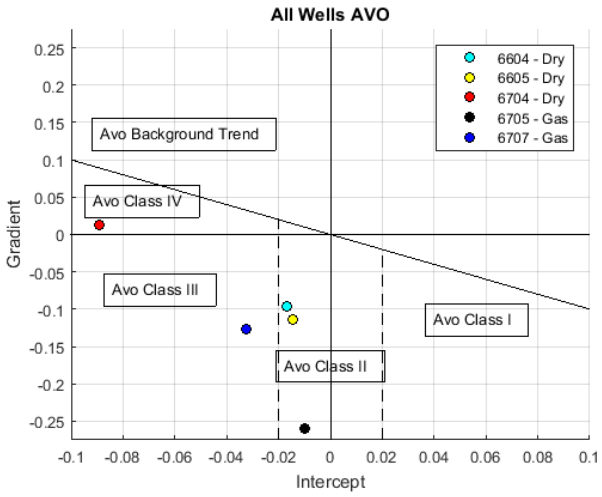

Figure 5.8: Calculation of Intercept and Gradient with AVO Classificaiton overlay

5.3.2 Stochastic AVO

The following section outlines the result from incorporating a stochastic modeling technique into the AVO modeling workflow. Figure 5.9 show a comparison between a normal AVO calculation using mean values on the left and on the right a set of values when using 1000 random numbers generated from the covariance matrix. The conclusions that might be drawn from the two images, can be quite different. In the simple mean calculation, well 6707 could be interpreted as being too close to the background trend of the 6604 and 6605 wells. However when using the stochastic plot it can be see that it has a huge range of possible values ranging from close the brine points to farther out in the Class III AVO area.

Figure 5.9 also shows that overall the 6707 and 6705 wells can be interpreted as strong Class II and Class III anomalies which lie far away from the background trend. The 6604 and 6004 are tightly clustered and do not show a significant change. Again well 6704 shows a different response when it comes to Gradient, in this case positive, resulting in a Class IV.

This highlights the benefit of using the stochastic method as it allows the full range of possibilities to be considered. It also shows that AVO, although historically based on a qualitative classification scheme could be considered through a probability estimate instead. Accuracy is a measure of data points being close to the true measure. In that context, the stochastic method proves more accurate as it is likely that the results are a better representation of the true values.

This method allows the entire data range, or just the percentiles to be visualized

depending on the need. Visualizing the percentiles gives a good indication of the range of the data without resulting in large overlap of points.

The second figure in this section, 5.10, shows a statistical representation of value used as input to the AVO and the output. Again, this figure is split in two. The plot to the left in figure 5.10 is a plot of Vp/Vs vs AI which shows the P10,P50 and P90 values for both overburden and reservoir for each of the wells. Secondly a plot of Intercept and Gradient shows the P10, P50 and P90 values for Intercept and Gradient calculated from the overburden and reservoir using the Shuey equation (2.2.3).

The 6707 well does show a large range of data points which are less well constrained than the other wells. This is shown in figure 5.11 which shows a comparison histogram for the input data from the 6605 and 6707 wells used by the covariance matrix and random number simulation.

The range of the data is approximately the same for the two data sets but the Vp of the 6707 well has a bimodal distribution. This come from the presence of prominent shale interbeds in the reservoir zone. The data sample from Well 6605 is a more homogenous sand which shows as a almost perfect normal distribution.

To correct for this effect of shale intervals the values could be sampled out based on a VShale cutoff. However, for the purpose of visualising the entire range of possibilities it can be more realistic to keep them in.

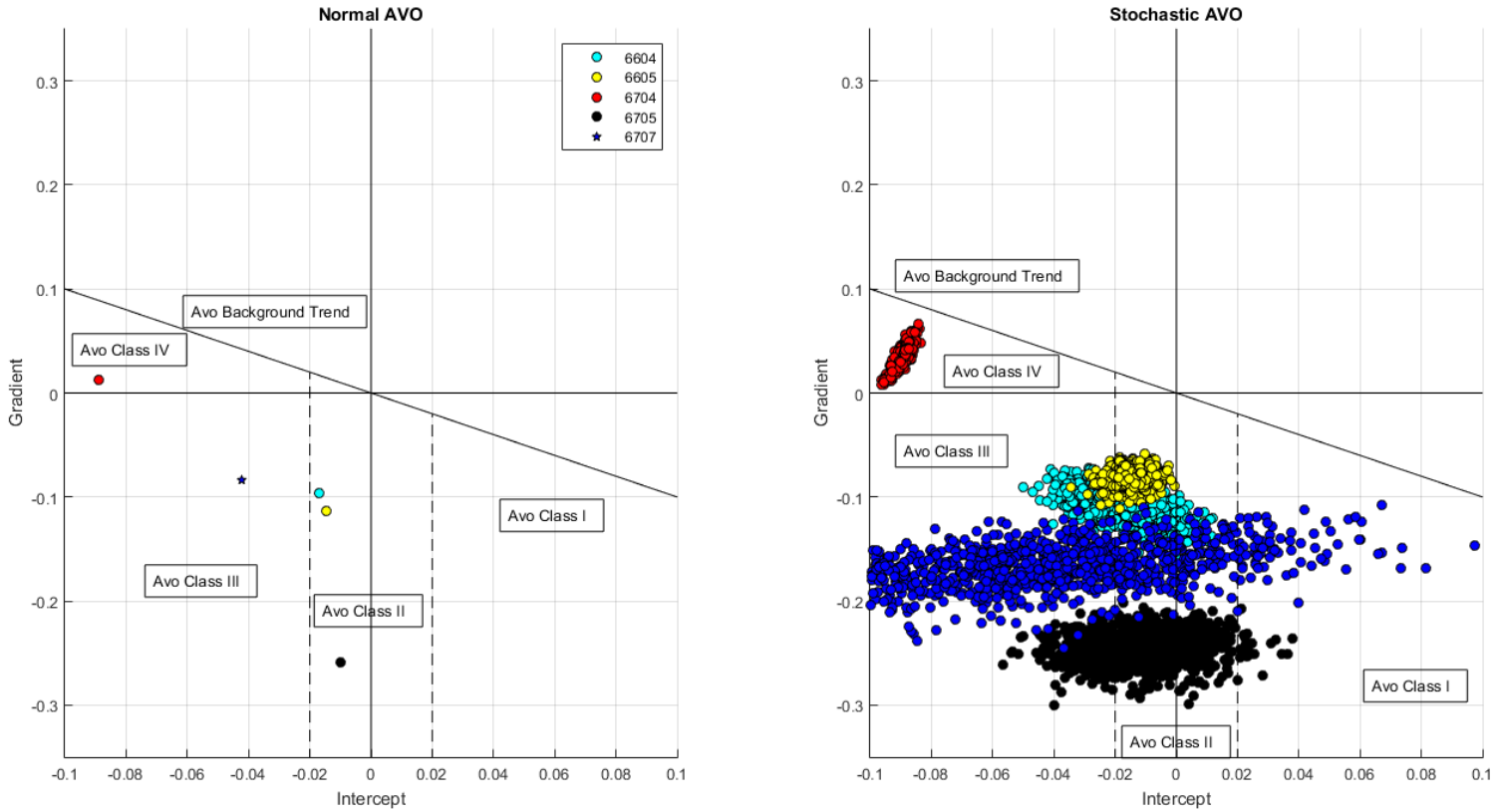

Figure 5.9: Intercept Gradient plot for normal average method and stochastic method

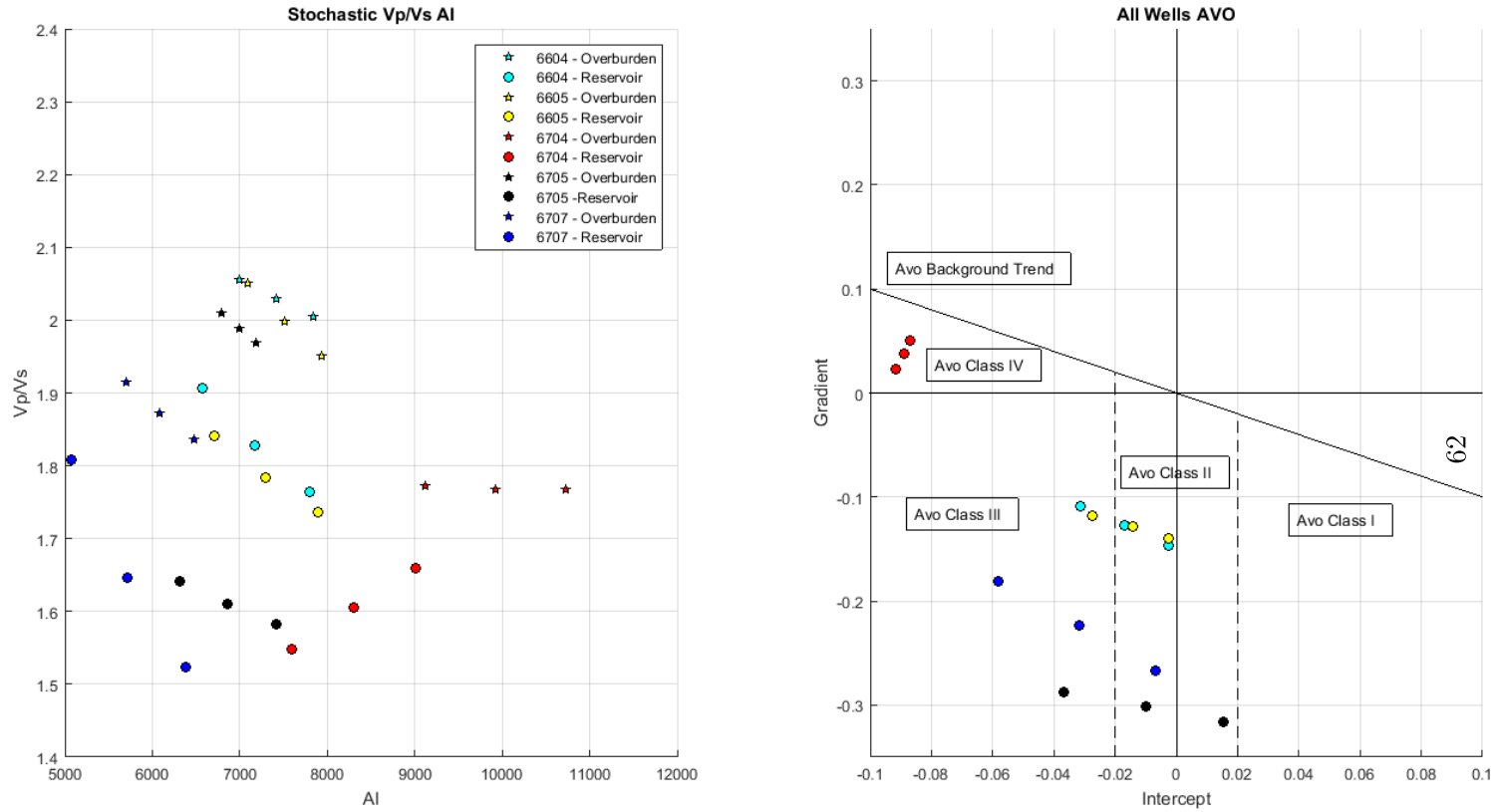

Figure 5.10: Calculation of Intercept and Gradient for 1000 random samples with AVO Classification overlay

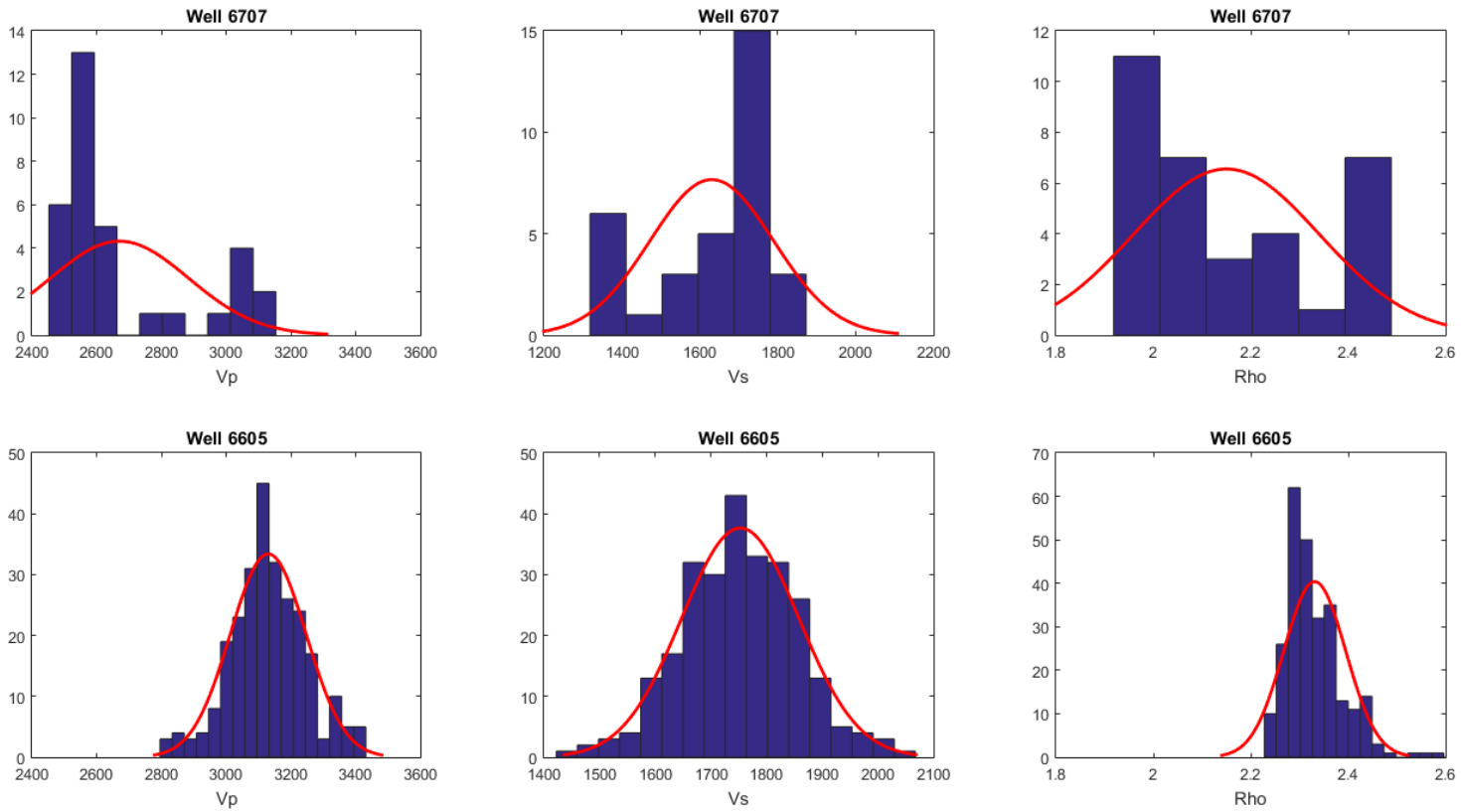

Figure 5.11: Histogram for 6605 and 6707 Vp,Vs and Rho

5.3.3 Fluid Effect on AVO

Figure 5.12 shows the result on AVO of fluid substitution, which was discussed in section 5.2. The original data points are shows as a circle and the substituted points as a star. In this case wells 6705 and 6707 are substituted Gas to Brine and the others Brine to Gas.

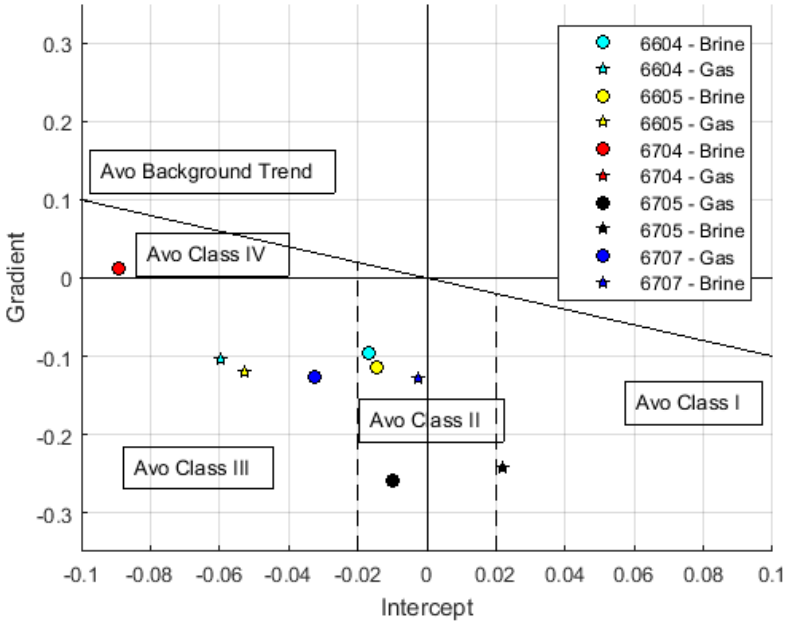

Figure 5.12: Plot of AVO response before and after fluid substitution

What can be observed form this data is that if a well contains hydrocarbons it should plot clearly in a strong Class II or Class III position. When brine was substituted in the well 6707 it plotted as a Class I and the well 6705 in Class II, but close to the original brine points of the other wells. By substituting all the wells in the study to brine a better estimate can be made about the limit between brine and gas reservoirs in terms of their AVO response. This can be roughly interpreted as an AVO background trend. This limit or trend is shown in figure 5.13 as a black dashed line.

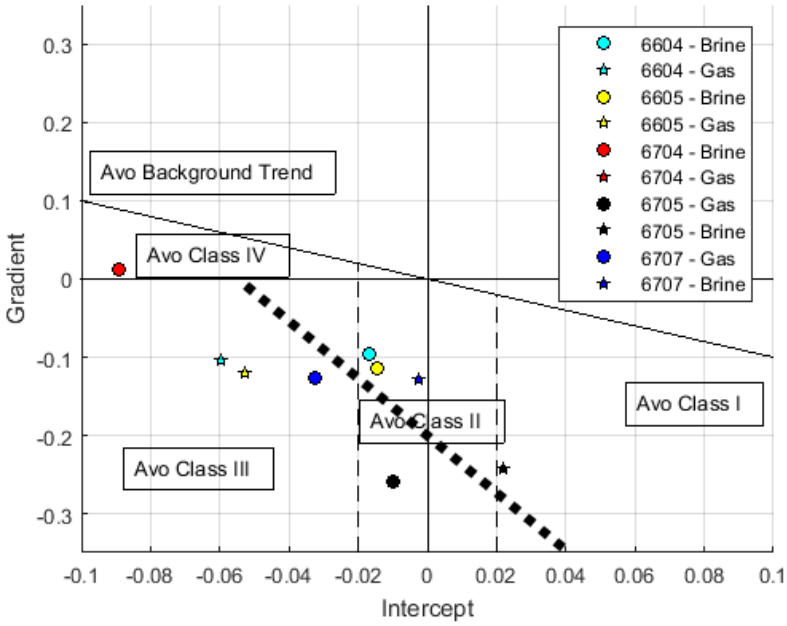

Figure 5.13: Plot of Fluid Substitution AVO with background trend

This technique shows that through AVO modelling of a set of wells from a particular area, a better estimation can be made of the background trend vs hydrocarbon trend for AVO classification.

In this example, when substituted with gas the well 6704 plots off the scale in a class III area but likely with a small negative Gradient. This highlights the fact that AVO strength should also be considered in addition to the classification scheme. Well 6704 when fluid substituted would appear as a Class III but not close enough to the other points to be considered a normal gas sand response. Hence, this method would highlight potential responses that would require a more detailed investigation.

5.4 Rock Physics

This section discusses the results from the rock physics modelling and overlaying models with the well data.

5.4.1 Gardner

Figure 5.14 shows the result of visualising the well data with Gardners model for sand and shale.

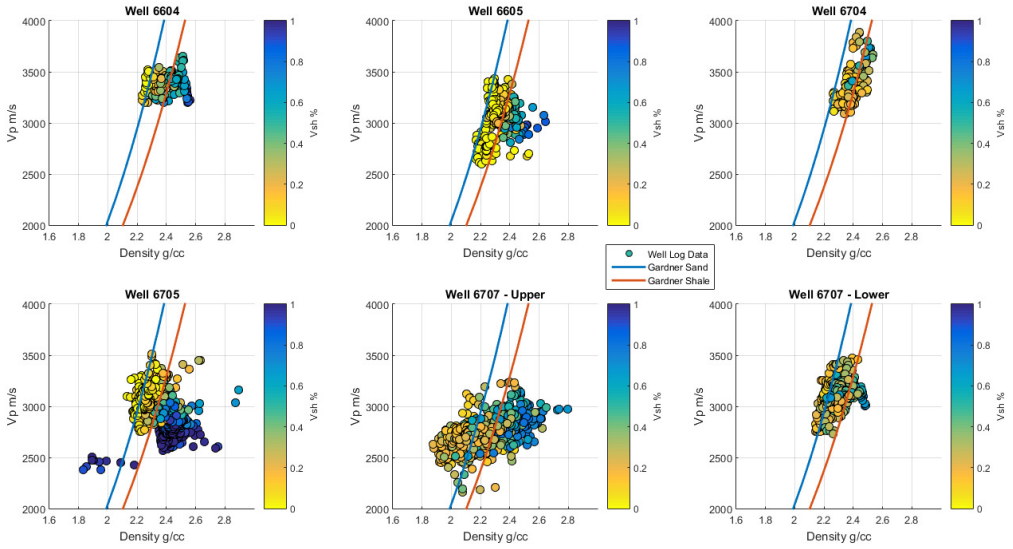

Figure 5.14: Raw Data with Gardner Sand and Gardner Shale Model

Other than as an indicator of sand against shale the Gardner models do not add any significant improvement to the interpretation of the raw data. It shows roughly for each well where the distinction between sand and shale should be. It also shows the wells where the distinction may be less clear and the change between sand and shale may be more gradational for example, in wells 6704. The 6705 and 6707 do show a clear distinction between sand and shale.

5.4.2 Han

Figure 5.15 and 5.16 shows the result of visualising the well data with the Han model for brine saturated sands. In figure 5.15 the data is coloured by VShale and in figure 5.16 by Porosity. The Han model is defined in terms of clay content and porosity.

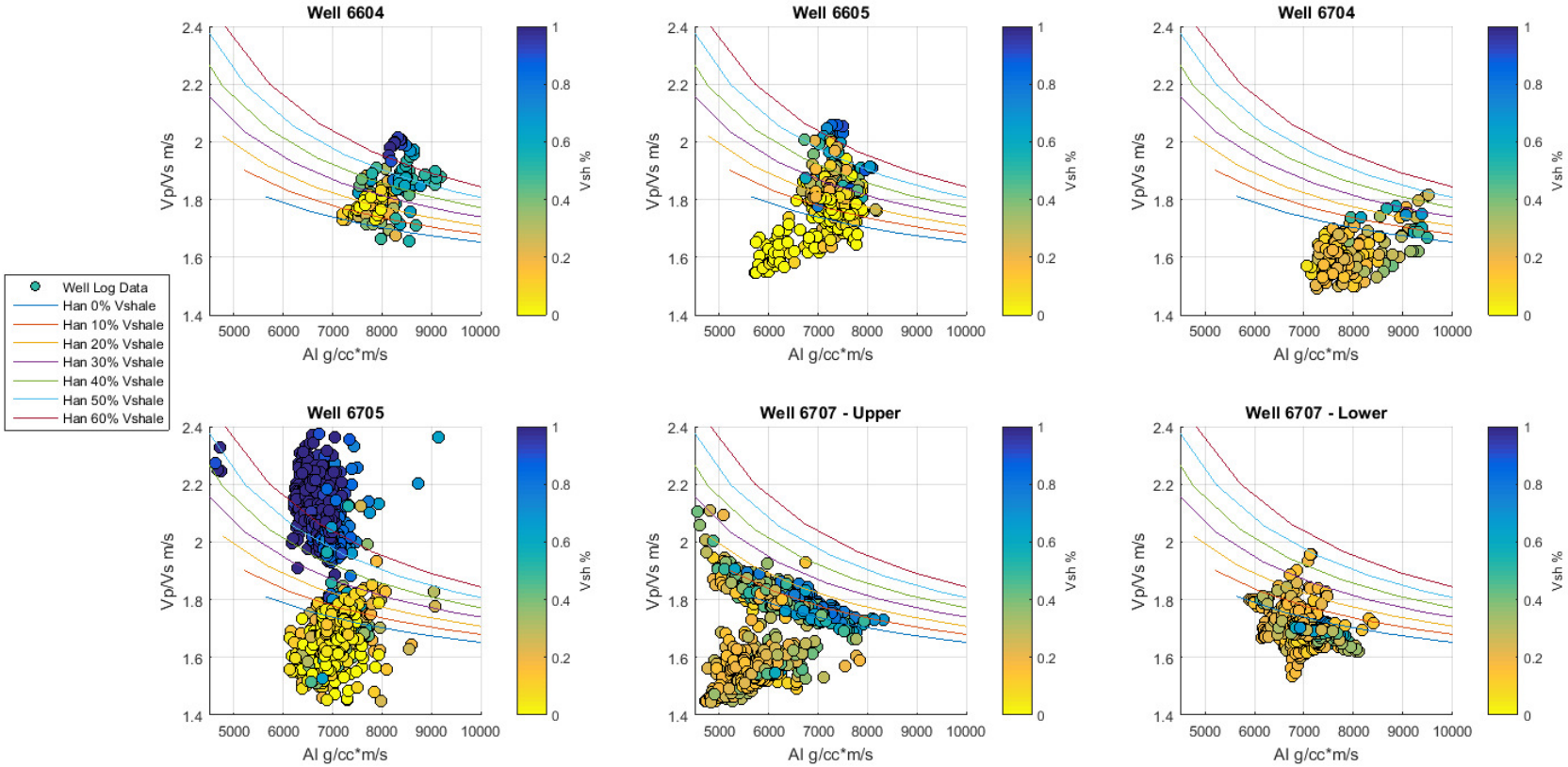

Figure 5.15: Han Model coloured by VShale

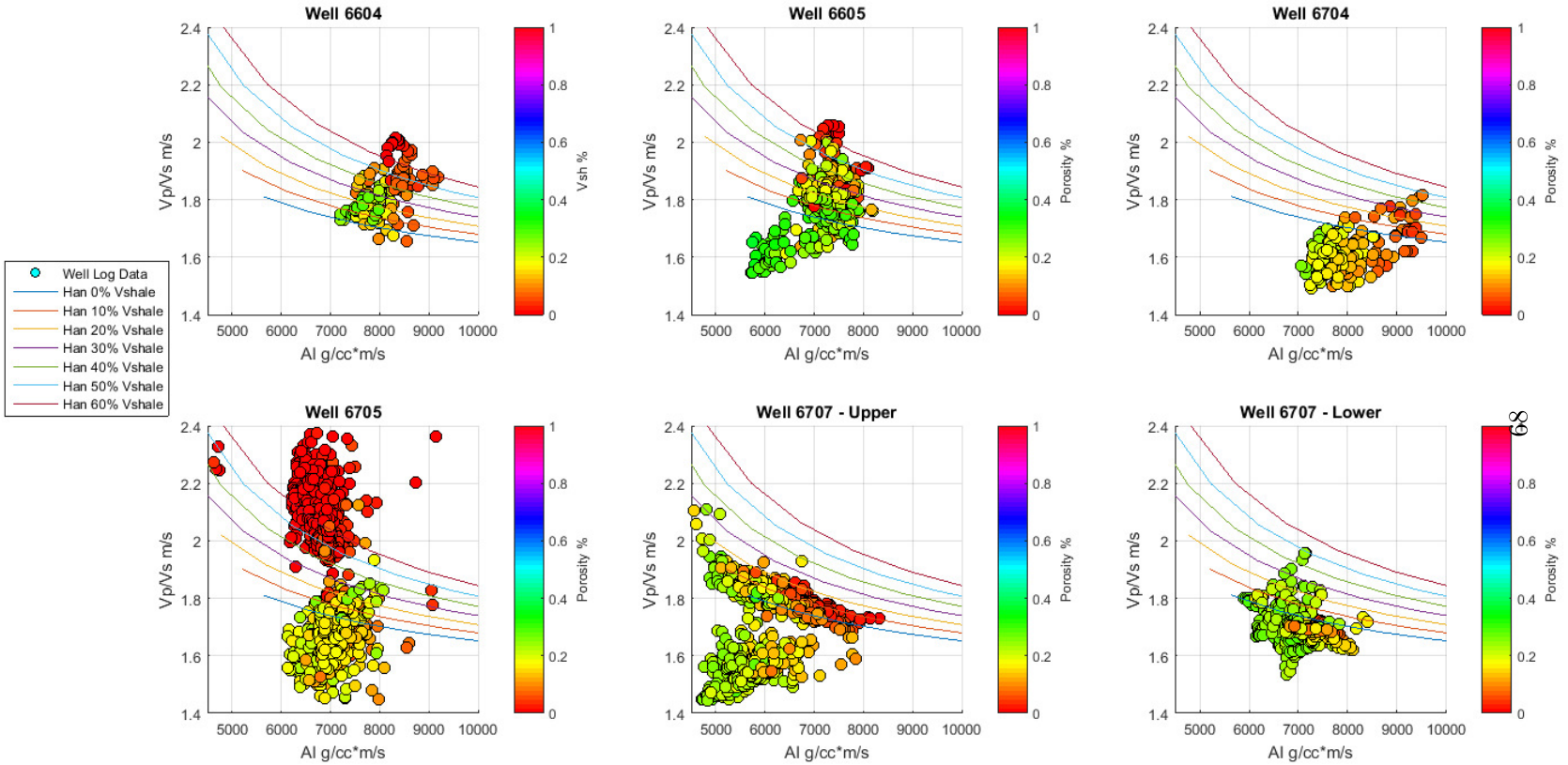

Figure 5.16: Han Model coloured by Porosity

The Han model shows two useful parameters which help in the interpretation of the data. Firstly, each line represents a model with a given amount of shale. Each line upwards represents and increase of 10 percent of shale from an initial 0. The Han model is also built using porosity which is increasing from left to right from 0 to 40 percent.

This model is based on brine, therefore sands which do not fit may be saturated with gas. Based on this model, it can be demonstrated that the well 6604 is likely a brine sand of moderate porosity. Well 6605 may contain some gas, but is likely mostly consisting of brine saturated sands of moderate porosity. Well 6704 is lower porosity but could indicate gas, however, given the larger depth of the reservoir it could simply be a pressure effect.

Well 6705 and 6707 are similar and show gas sands plotted lower down and away from the model.

The second plot of the Han model is coloured by porosity. In this case it shows that although the model fits the overall trend of the data(lower porosities to the right),the absolute values are a poor match for the Han model. This would make the Han model unsuitable for porosity prediction purposes.

5.4.3 Constant Cement

Figure 5.17 shows a plot of the AI against VpVs for each of the wells in the study. This is done as a calibration step to ensure that the model fits the data and can be further used. The reservoir units found in the 6705 and 6707 wells are interpreted to be clean channel sands which are thicker and more homogenous than in the other wells.

In addition, two series of data representing the limits of the Constant Cement model are added. The model consists of two main lines represented by the labelled points, 1) an upper 100% brine line of varying porosity 2)a lower 100% gas line of varying porosity. This model allows the effect of both saturation and porosity to be modeled in one expression.

The two lines appear to fit the data reasonably well in terms of fluid saturation i.e. most of the sand points plot in the middle or around the model. Some points however do not fit the model very well, plotting further down to the lower left. This could be due to having a different cement scheme than the other reservoirs or due to difference in the fluid properties, even though the same fluid parameters have been used. The result of using these points to calculate reflectivites for varying porosity and saturation is discussed in the section below.

Reflectivity Models

Figure 5.18, which is divided into four plots, gives an overview of the reflection modelling of the constant cement model. The upper left plot is a plot of VP/VS against AI which shows the brine and gas for varying porosity from the constant cement model. The colours represent pairs of porosity, whereas the fill represents gas and the non-filled points brine. Figure 5.18 shows that the Vp/Vs Ratio for varying porosity with constant brine saturation changes significantly whereas for gas saturated points, Vp/Vs changes less. This plot also shows that at lower porosities the effect of gas rather than brine is less on the Vp/Vs ratio.

The upper right plot contains an intercept and gradient plot for each of those points. From this plot it can be seen that the mid-range porosity gas points more or less correspond with a Class I, Class II and Class III AVO. The brine points also follow this trend but track close to the background trend. The upper right plot also illustrates that it might be hard to distinguish between a low porosity brine sand and gas sand.
The final two plots describe the reflectivity of the different porosities for brine (left) and gas (right). These plots show that the effect of substituting brine with gas, shifts all reflections down on the Y-Axis towards negative Intercepts. This plot shows that only porosities of 20% or above exhibit the negative intercept and negative gradient that is normally associated with gas bearing sands. Again, these plots highlight the ambiguity or overlap that can occur between brine and gas sands of different porosities. The plot shows that brine saturated sands almost always have a negative gradient but can also have a positive or slightly negative intercept. Gas Saturated point also have mostly negative gradient but have low positive and high negative intercepts.

This process of forward modelling from a rock physics model mirrors the AVO response from the raw data but benefits from the fact that additional properties i.e porosity can be linked to changes in Intercept and Gradient.

Figure 5.19 shows a simple synthetic for a model of overburden, reservoir and underburden for each data point in the constant cement model. An average background shale is used as the overburden. This produces a plot for different porosities for both gas and brine.A number of different elements can be seen from this matrix. Firstly, the overlap between the response of brine sand of 25% porosity and Gas sand of 15%, as these two reflections have a very similar response. They also exhibit a phase reversal in both cases which is an amplitude moving from positive to negative. From 20% and above the gas sands exhibit normal behaviour which is a negative response with an increase (becoming more negative) with offset This is particularly clear on the gas sand 20% porosity. The gas sand with 20% is a typical AVO reflection becoming stronger/brighter with higher offsets.

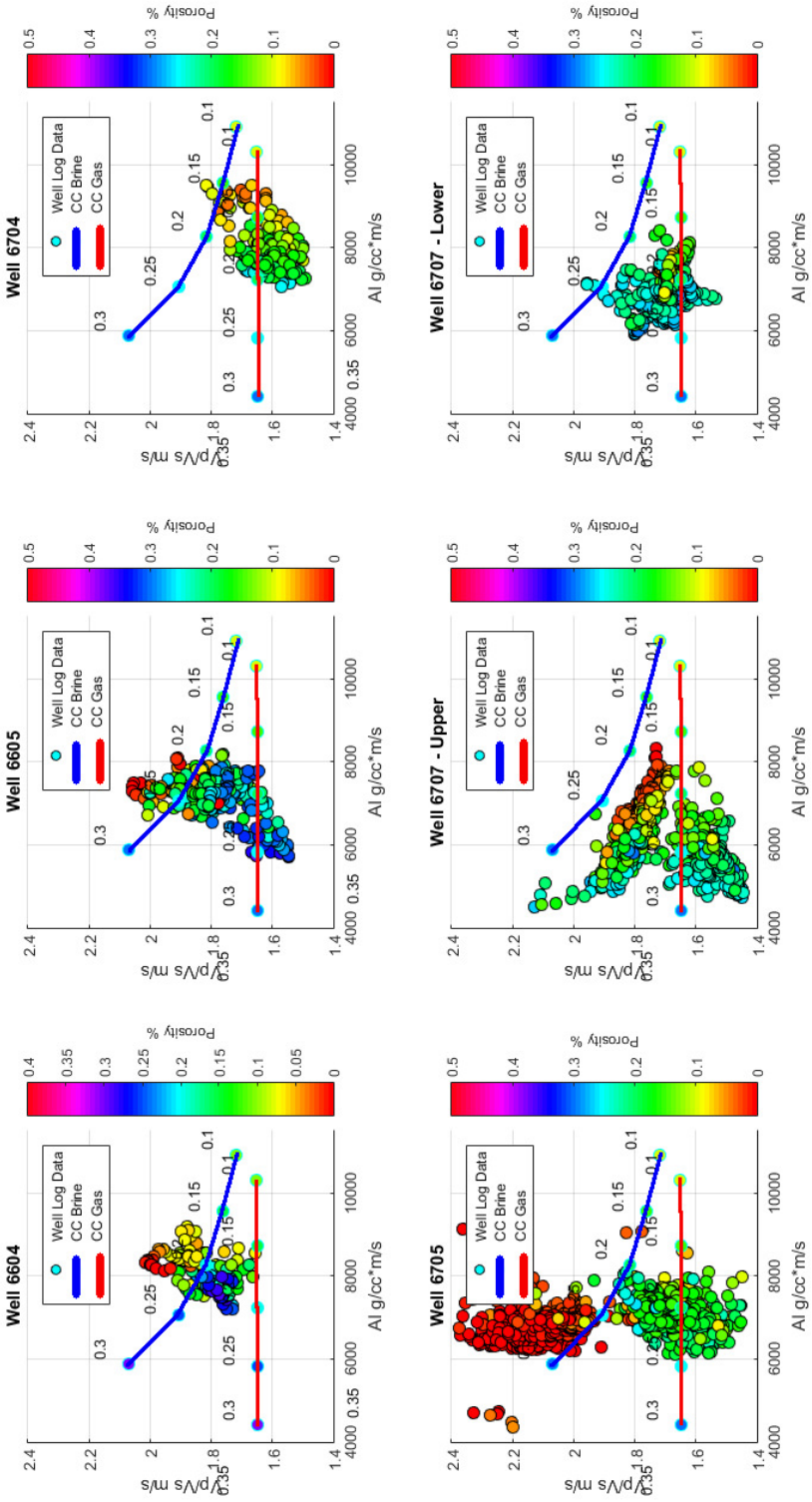

Figure 5.17: Raw Well Data with Constant Cement Model showing Brine and Gas

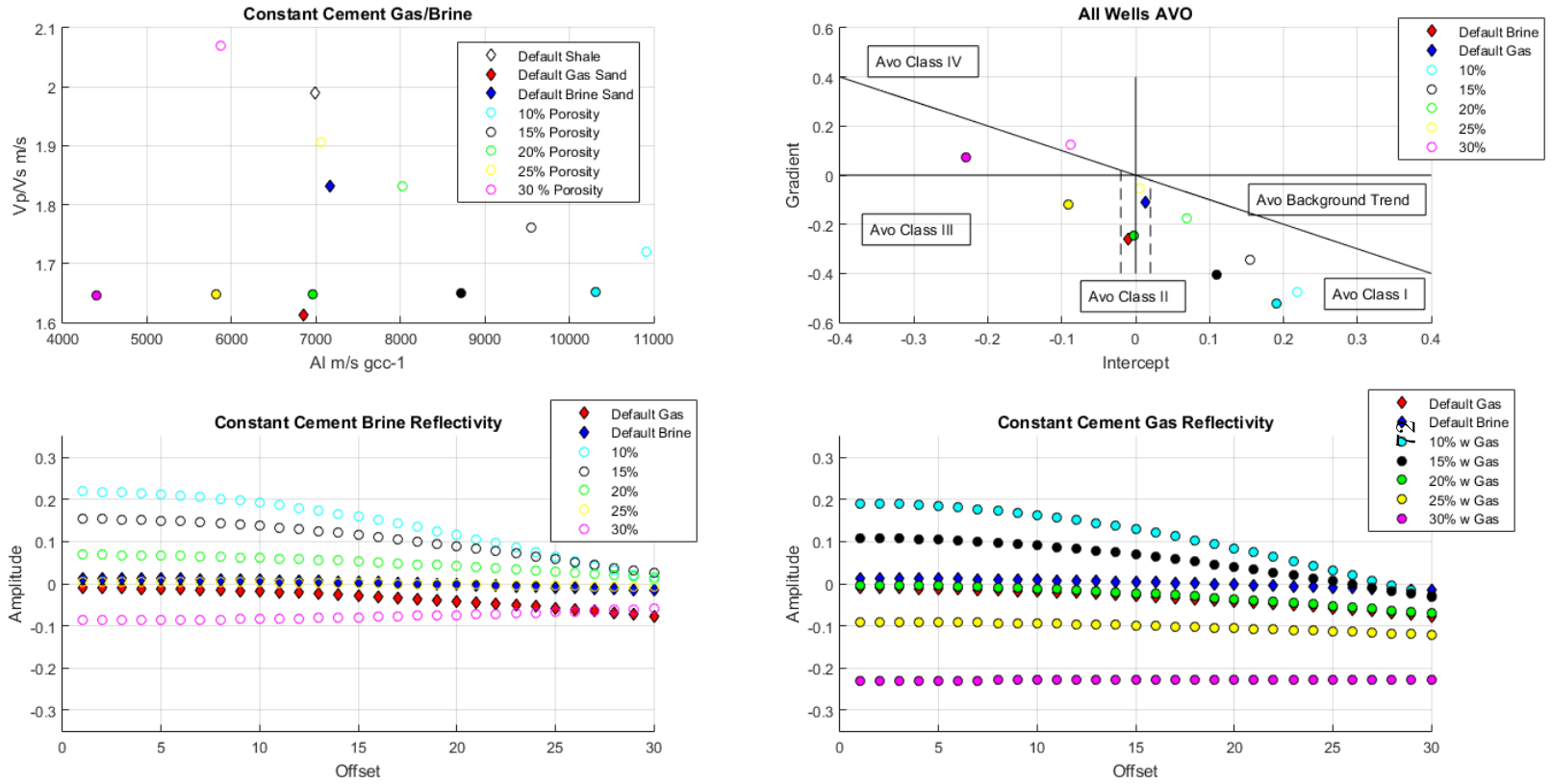

Figure 5.18: Reflectivity for 10 to 30 Porosity Brine and Gas

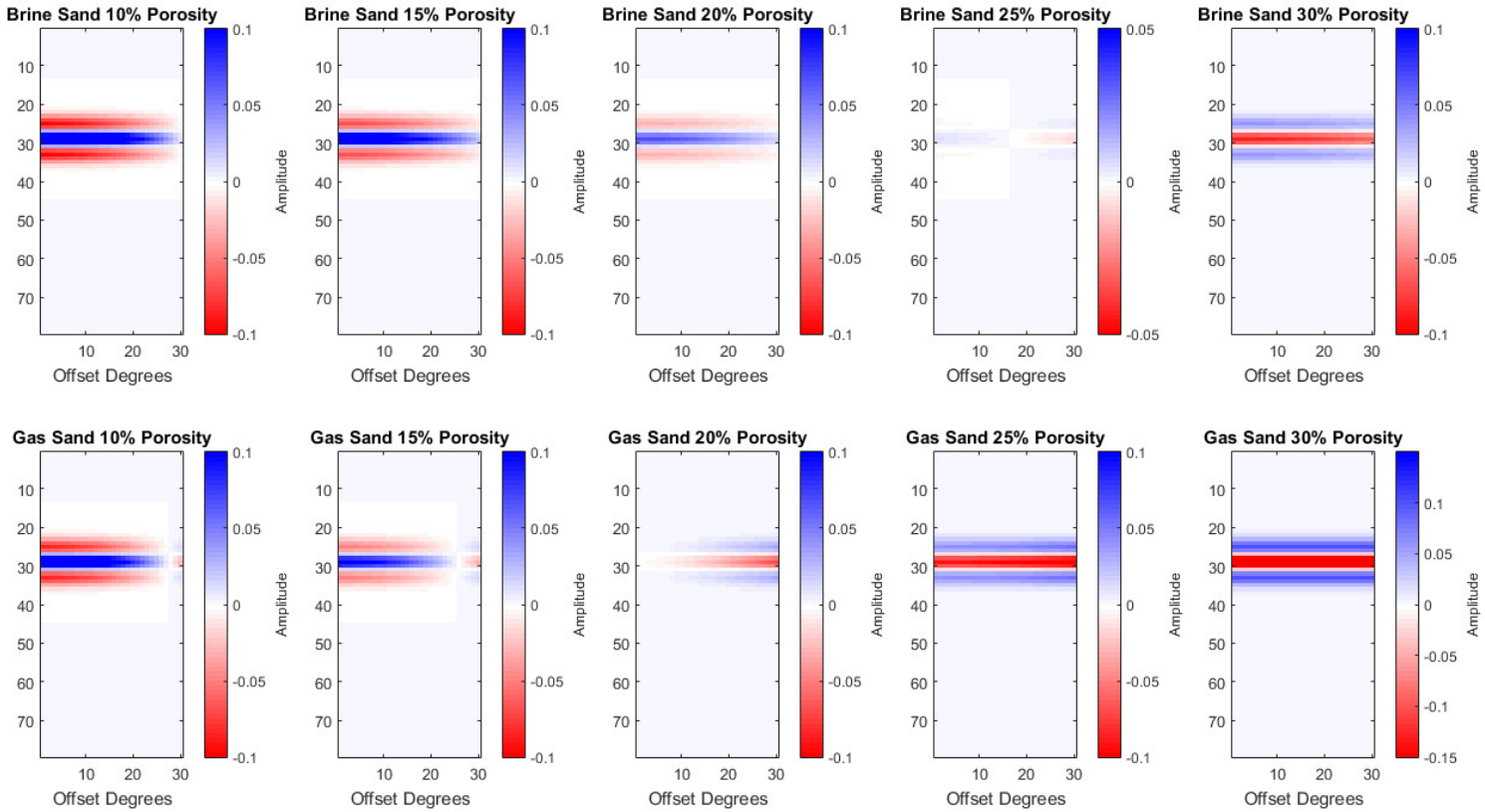

Figure 5.19: Synthetics Seismic Model for 10 to 30 Porosity Brine and Gas

5.5 AI GI Cross plots

The AIGI cross plots allow a direct estimation of impedance changes to be related to changes in the geology. The X-Axis reflects relative changes in Intercept Impedance, which equates to acoustic impedance, and the Y-Axis relative changes in Gradient Impedance. The colour distinguishes different properties which can be related to these trends. In the 6705 well, figure 5.5, i can be observed that the changes from high VShale in blue to low VShale in yellow would result in a large negative gradient. Whereas well 6605 would be characterised by large changes in Intercept as the direction of separation is largely along the X-Axis.

When combined with figure 5.21 it is possible to interpret the response in both terms of sand against shale and brine against gas. With both properties in consideration the well 6705 hydrocarbon sands would be classified by a negative intercept and large negative gradient, which agrees with the earlier reflectivity calculations. In this figure, well 6707 also exhibits a large change in both intercept and gradient between brine sand and gas sand. This plot proves quite useful particularly because it can be coloured by any property to give an idea of how that property relates to the Impedance changes.

Well 6704 also agrees with earlier estimation of a positive Gradient between Sand and shale with a negative Intercept.

The downside of this plot is that some of the properties are less well separated out making interpretation more difficult. In well 6705, for example, the points of low to medium Sw are tightly clustered and it is difficult to infer anything about the impedance changes between brine and gas sands.

5.6 EI Results

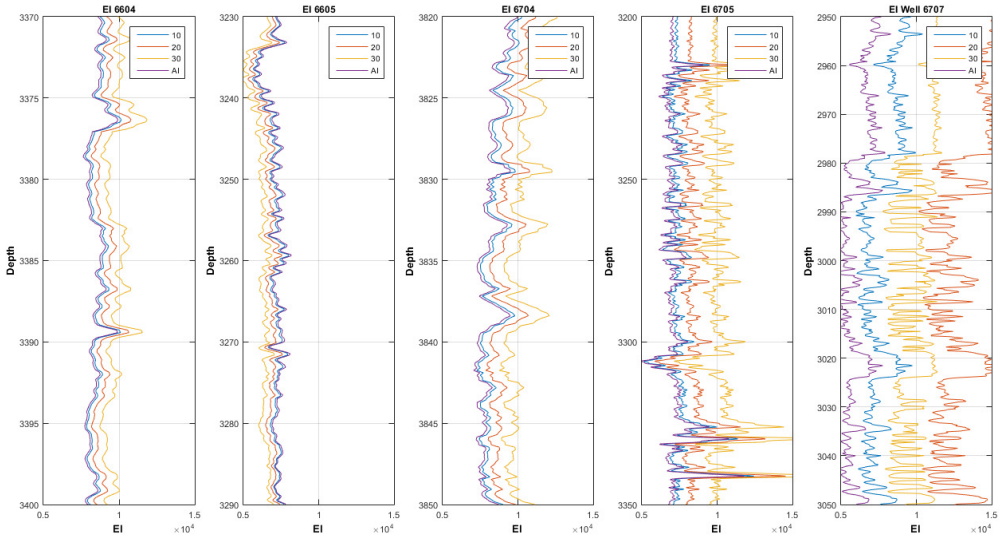

Figure 5.22: EI Logs for each well at 10, 20 and 30 degrees offset

Figure 5.22 shows an estimation of the Elastic Impedance or EI for each reservoir zone for offset angles of 10,20 and 30 degrees. These results show which wells have a strong change in Elastic Impedance with offset, well 6705 and 6707. Wells 6004 and 6704 have a small change with offset. Well 6605 has a negative change with offset which means the EI is decreasing. EI is a method to simulate the impedance with offset to understand how the impedance will behave at specific amplitudes. These angles were chosen as an approximation for Near, Mid and Far, however, any angle may be chosen. The calculation can help to show how the impedance changes with offset. In practice, this can only be used as a control on the seismic to give an understanding of the main contrasts at a particular angle.

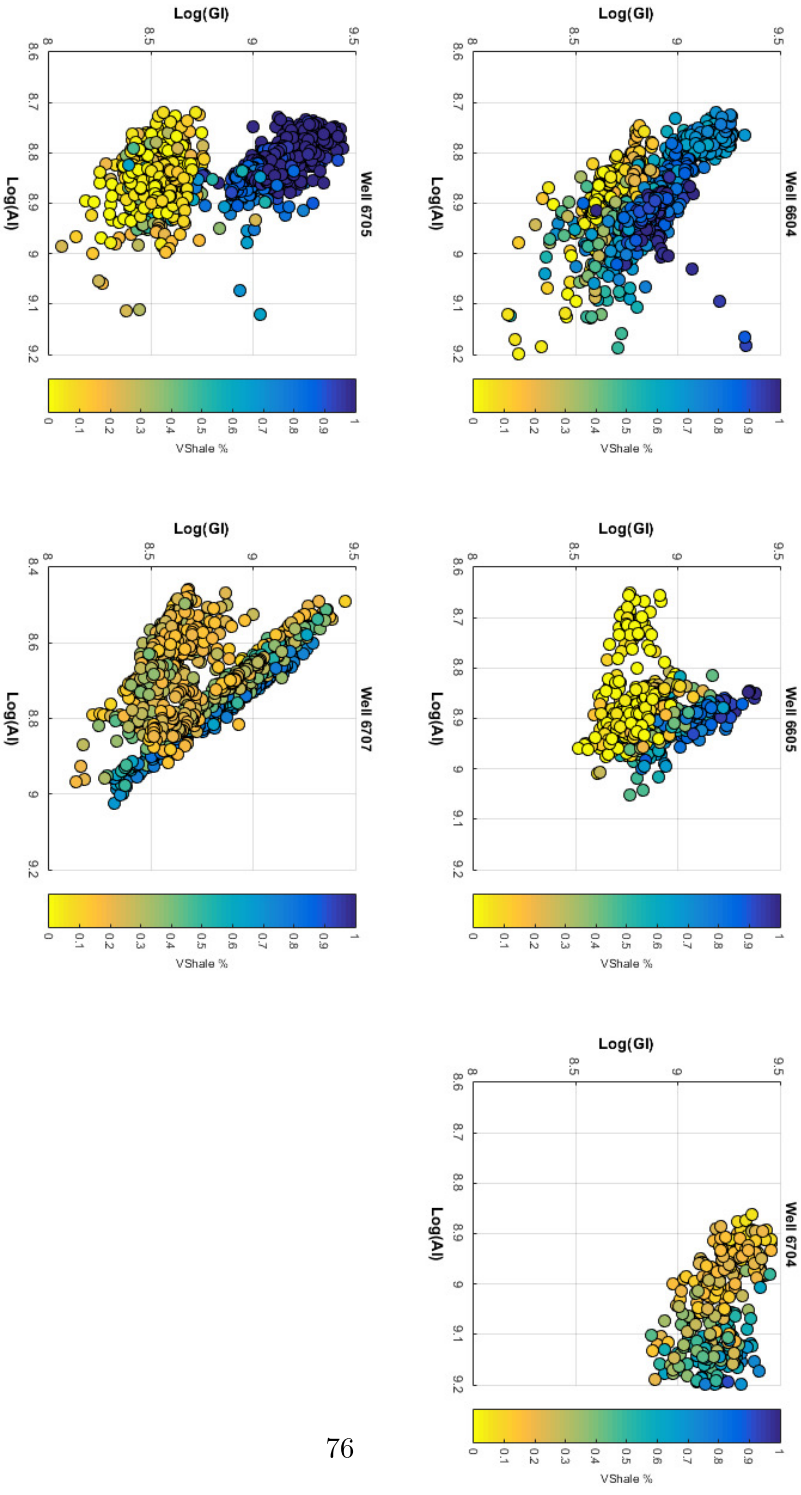

Figure 5.20: AI vs GI coloured by VShale

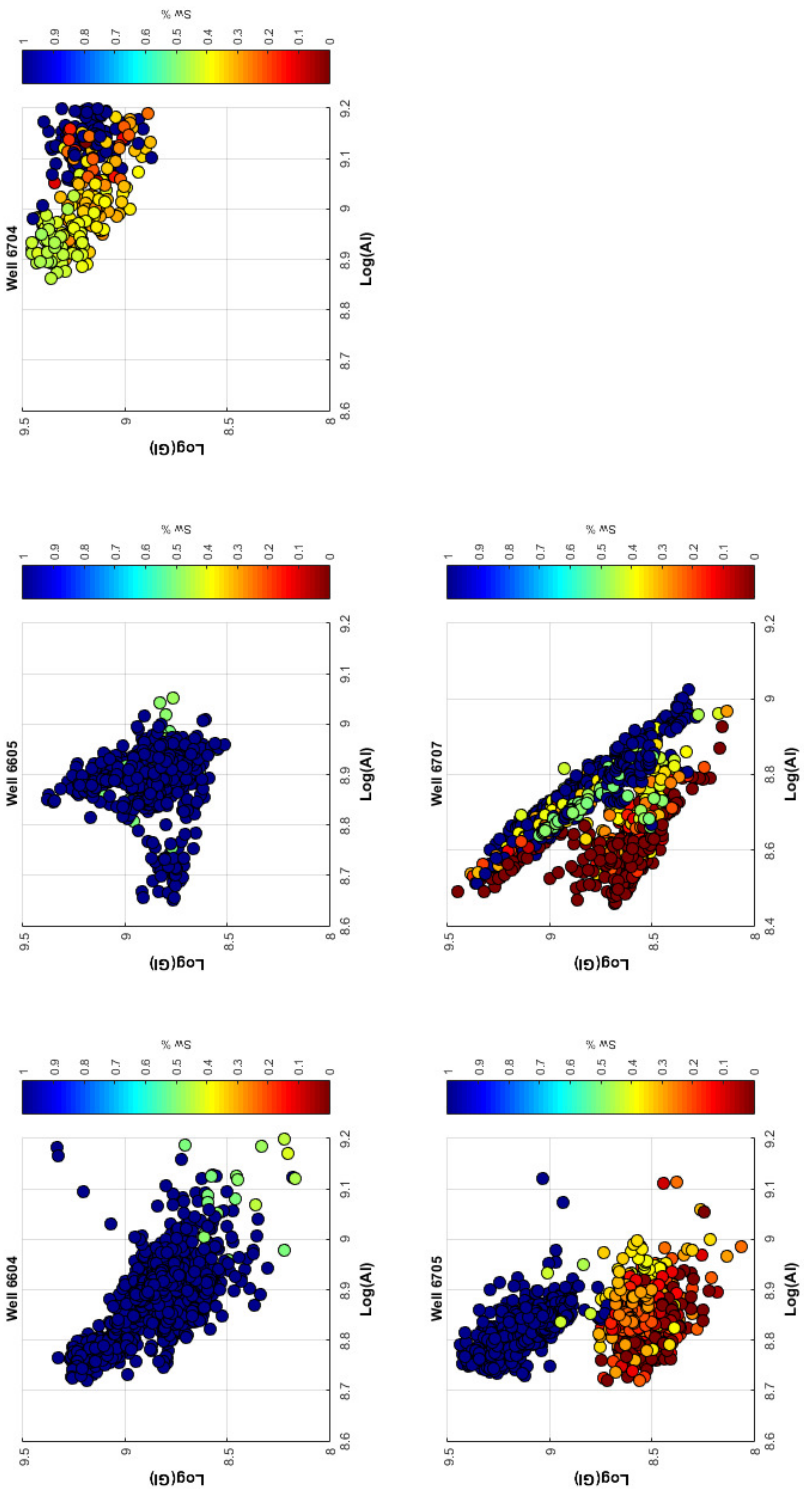

Figure 5.21: AI vs GI coloured by Sw

Chapter 6

Conclusions, Discussion and Further Work

This chapter outlines the main findings and conclusions of this study and makes recommendations for further work. This study has focused on deep marine environment of the Vøring Basin. Conclusions are applicable for other deep marine environments and likely applicable for other clastic environments. Other environments such as shale plays or carbonates should be approached differently.

6.1 Conclusions

This study highlights that integrating AVO, forward modelling and impedance techniques allow for a more robust approach for linking geological observables to the seismic response. This study also highlights that interpretation and petrophysics, in particular porosity estimation, underpins many of the subsequent techniques.

In conclusion, an integrated approach to AVO and reservoir characterisation is an effective way to gain a better understanding of the role that different geological controls have on the seismic response in a particular geological setting such as the Vøring basin. Combining traditional AVO classification with impedance techniques can improve the ability to distinguish hydrocarbon bearing sands from non-reservoir. This approach also helps to understand how increasing amounts of VShale will effect the expected AVO response.

The main conclusions from the study are as follows:

- Simple AVO classification, based on averaging, is not sufficient enough to definitively

identify a hydrocarbon response

- Highlights that in addition to AVO Classification, considering general reflection behaviour and AVO strength can help to identify hydrocarbon vs dry reservoirs

- Shows that using an AVO classification scheme in conjunction with a stochastic method can improve ability of the scheme to identify hydrocarbon vs dry reservoirs

- Impedance plots such as AIGI provide a convenient scheme with which to directly relate geological properties to the seismic response

- When detailed knowledge of fluid and mineral properties are available, Fluid substitution is an effective way to model the seismic response to fluid changes

- Rock physics models, when poorly correlated, can only be used to show relative changes in seismic related to geological properties

6.2 Research Questions

Do the reservoir rocks from the Vøring Basin exhibit consistent AVO / elastic behaviour?

Based on the five wells in the study the wells from the Vøring basin appear to exhibit AVO behaviour that is consistent with the background theory. Gas sands show as Class II and Class III AVO with a significant deviation from the background trend. Brine saturated sands of the same porosity shows as a similar class but much closer to the background trend. This highlights the fact that AVO strength as well as class is an important factor in distinguishing hydrocarbons from brine.

One well deviates from the four by having a Class IV response but this is mostly related to the change in acoustic properties with the overburden rather than the reservoir properties. This well is at a greater depth than the other wells and thus may have a more compacted overburden or contain a higher cement volume in the sand.

To what extend does the geological environment influence the elastic properties of the rocks?

In the five wells the biggest factor in AVO response is primarily related to fluid saturation of brine vs gas. Modelling of porosity also showed that changes in porosity have a significant effect on the AVO response. This confirms the observation that porosity changes can result in an overlap in AVO response between Gas sands and Brine sands with a higher porosity.

The results of this study also show that depth of the reservoir, which influences properties such as compaction and cement volume, is an important control on the elastic properties. The relationship between overburden and reservoir can change significantly at varying depths. This is most prominent in the 6704 well where the overburden properties are different from that of the other wells. This may be due to compaction as the well is at a greater depth.

How effective are current methods to model changes in elastic properties?

The impedance approach from Connolly (1999) and Florez and Kuzmin (2015), offers a convenient way to related geological properties to elastic or seismic properties as the AIGI plot can be coloured by potentially any property. The downside of this being that the plot may not separate out certain features as well as the traditional Vp/VS AI plot.

Traditional AVO classification is not very effective at modelling changes in elastic properties but can be improved through the use of stochastic modelling. When detailed fluid and mineral properties are known fluid substitution is an effective way of modelling the fluid effect. Modelling of different porosities on the seismic can be done using a rock physics model, but when there is a poor fit between model and data the results can only be used to compare the relative response.

How to better distinguish hydrocarbon bearing sands from non-reservoir using AVO modelling techniques?

Considering AVO strength as well as AVO class is an important way to quality control the AVO interpretation scheme. This was also confirmed using a stochastic modelling method for AVO classification which helped to shows the range of possible values. By integrating fluid substitution into this process a measurement can be made on the AVO background trend or strength profile that can distinguish hydrocarbons from brine.

6.3 Discussion and Further Work

Outlined in the methodology is the process of calculating AVO for each Well for pairs of overburden and reservoir measurements. In this study, it was decided to keep the analysis on a well by well basis in order to link back to the original observations made in each well. An alternative approach to this methodology, which is followed by Avseth et al. (2005), is to group the data from each well together into a larger data set and then divide back per each distinct facies i.e. brine sand, gas sand, shaley sand etc. This would allow an alternative form of scenario testing and modelling to be done as different combinations of facies and overburden could be considered. This method could be preferred if there was more variation in the data than was observed with the five wells.

The AVO calculation for each well included an estimation of the Vp,Vs and Rho for overburden and reservoir for each well. From this a reflection series was calculated and an AVO response estimated. The results for each well was then compared. This approach does not consider variations in the overburden which could also cause differences in the AVO. The overburden for four of the five wells was deemed to be consistent with some difference being observed on the 6704 well. As discussed in the results this well is at a much larger depth which can change the elastic properties of the shales significantly.

These two issues could be addressed in further work, but taking a different approach to the modelling and instead using facies groups instead of a well by well basis.

The rocks physics models used for porosity modelling have a number of assumptions when used. The contact cement model was calibrated once to fit the general reservoir sands of the area. This model however assumes that the amount of cement in the rocks is constant. As the rocks were over a similar depth range this was deemed a relevant choice. This however limits the scope of the modelling to be only valid for the same depth range. Further work could also take into account depth variation as an additional variable. This would have large implications for the rock physics part of the study as well as the AVO results.

Elastic Impedance offers a way of understanding the Impedance change with offset, but does not offer much insight to prediction of fluid or lithology. This contrasts results shown by Connolly (1999) and Whitcombe et al. (2000). In this case however, it may have not proved the best result as the wells were from different parts of the basin rather than from a single prospect or field. This technique should also be used as a comparison with the seismic data rather than as a comparison between wells.

Future reservoir characterisation studies can make use of the techniques discussed in this study. Firstly, a more detailed approach to AVO analysis can yield more reliable results

and build a better understanding of the reflection behaviour. In this study, stochastic techniques improved the simple AVO classification scheme but could be expanded more towards fluid substitution and rock physics. Stochastic approaches to rock physics and inversion techniques are emerging and described by authors such as Manuel Cobos and Castanga (2014) and Johansen et al. (2013).

Another area not fully explored by this study is the effect that petrophysics has on techniques such as fluid substitution and rock physics modeling. In this study standard transformations where used to predict properties from the raw wireline logs. These assume that the logs are good quality and consistent across all wells. Future studies may wish to explore further the sensitivities of fluid substitution or rock physics to changes in petrophysical estimation. Water Saturation and Porosity can be estimated in different ways depending on the situation.

To further extend this study, seismic data from the Vøring basin could also be acquired to fully explore the AVO behaviour and results from seismic data. This would enable the Elastic Impedance, Connolly (1999) approach to be properly assessed and in addition make use of the Extended Elastic Impedance approach from Whitcombe et al. (2000). This approach assumes that by applying a rotation to Intercept and Gradient there can be found an angle which discriminates hydrocarbon from non-hydrocarbons or discriminates sand from shale. This method is convenient as it does not require any forward modeling, but may be difficult to constrain if there is limited well data available.

References

ADEOTI, L., ADELEYE, K.O., ITSEMODE, A. and BELLO, M.A., 2015. Fluid prediction using AVO analysis and forward modelling of deep reservoirs in Faith Field, Niger Delta, Nigeria. Arabian Journal of Geosciences, 8(6), pp. 4057-4074

AKI, K., 1930-2005. Quantitative Seismology (2nd Edition). University Science Books.

AVSETH, P. and ODEGAARD, E., 2004. Well log and seismic data analysis using rock physics templates. FirstBreak, 22(10), pp. 37-43

AVSETH, P., DVORKIN, J., MAVKO, G. and RYKKJE, J., 2000. Rock physics diagnostic of North Sea sands: Link between microstructure and seismic properties. Geophysical Research Letters, 27(17), pp. 2761-2764

AVSETH, P., 2010. Explorational Rock Physics - The Link Between Geological Processes and Geophysical Observables. NEW YORK; 233 SPRING STREET, NEW YORK, NY 10013, UNITED STATES: SPRINGER.

AVSETH, P., MUKERJI, T. and MAVKO, G., 2006; 2005. Quantitative seismic interpretation: applying rock physics tools to reduce interpretation risk. Cambridge: Cambridge University Press.

AVSETH, P., MUKERJI, T., MAVKO, G. and GONZALEZ, E., 2007. Integrating Statistical Rock Physics and Sedimentology for Quantitative Seismic Interpretation. Subsurface Hydrology: Data Integration for Properties and Processes, 171, pp. 45-60

AVSETH, P., SKJEI, N. and SKALNES, A., 2013. Rock physics modelling of 4D time-shifts and time-shift derivatives using well log data a North Sea demonstration.

Geophysical Prospecting, 61(2), pp. 380-390

BACHRACH, R., OSYPOV, K., NICHOLS, D., YANG, Y., LIU, Y. and WOODWARD, M., 2013. Applications of deterministic and stochastic rock physics modelling to anisotropic velocity model building. Geophysical Prospecting, 61(2), pp. 404-415

BØIRLYKKE, K. and AVSETH, P., 2010. Petroleum geoscience: from sedimentary environments to rock physics. Berlin ; London: Springer.

CARMICHAEL, R., 1988. Practical handbook of physical properties of rocks and minerals. 1st ed. CRC Press.

CASTAGNA, J.P., SWAN, H.W. and FOSTER, D.J., 1998. Framework for AVO gradient and intercept interpretation. Geophysics, 63(3), pp. 948-956

CHI, X. and HAN, D., 2009. Lithology and fluid differentiation using a rock physics template. The Leading Edge, 28(1), pp. 60-65

CONNOLLY P., 1999. Elastic impedance. The Leading Edge, 18(4), pp. 438

DATTA GUPTA, S., CHATTERJEE, R. and FAROOQUI, M.Y., 2012. Rock physics template (RPT) analysis of well logs and seismic data for lithology and fluid classification in Cambay Basin. International Journal of Earth Sciences, 101(5), pp. 1407-1426

DVORKIN, J. and NUR, A., 1996. Elasticity of high-porosity sandstones: Theory for two North Sea data sets. Geophysics, 61(5), pp. 1363-1370

FAN, F. and MA, J., 2011. AVO Modeling for Coal Seam Prediction. Procedia Earth and Planetary Science, 3, pp. 138-143

FENG, Q., JIANG, L., LIU, M., WAN, H., CHEN, L. and XIAO, W., 2014. Fluid substitution in carbonate rocks based on the Gassmann equation and Eshelby–Walsh theory. Journal of Applied Geophysics, 106, pp. 60-66

FJELLANGER, E., SURLYK, F., WAMSTEEKER, L.C. and MIDTUN, T., 2005. Upper cretaceous basin-floor fans in the Vøring Basin, Mid Norway shelf. Norwegian

Petroleum Society Special Publications, 12, pp. 135-164

FLOREZ-NINO, J. and KUZMIN, S., 2015. Rock Physics Templates in AI-GI and Extended Elastic Impedance Domains. Society of Exploration Geophysicists.

GARDNER, G.H.F., GARDNER, L.W. and GREGORY, A.R., 1974. Formation Velocity and Density - This disagnostic basics for stratigraphic traps. Geophysics, 39(6), pp. 770-780

GOLIKOV, P., AVSETH, P., STOVAS, A. and BACHRACH, R., 2013. Rock physics interpretation of heterogeneous and anisotropic turbidite reservoirs. Geophysical Prospecting, 61(2), pp. 448-457

GUPTA, S.D., CHATTERJEE, R. and FAROOQUI, M.Y., 2012. Rock physics template (RPT) analysis of well logs and seismic data for lithology and fluid classification in Cambay Basin. International Journal of Earth Sciences, 101(5), pp. 1407-1426

HAN, D., NUR, A. and MORGAN, D., 1986. Effects of porosity and clay content on wave velocities in sandstones. Geophysics, 51(11), pp. 2093-2107

IVANOVA, A., BERGMANN, P., KUMMEROW, J., YANG, C., LÜTH, S. and JUHLIN, C., 2013. Seismic Modeling of the AVO/AVA Response to CO2 Injection at the Ketzin Site, Germany. Energy Procedia, 40, pp. 490-498

JOHANSEN, T., JENSEN, E., MAVKO, G. and DVORKIN, J., 2013. Inverse rock physics modeling for reservoir quality prediction. Geophysics, 78(2), pp. M1-M18

KING, M.S., 2009. Recent developments in seismic rock physics. International Journal of Rock Mechanics and Mining Sciences, 46(8), pp. 1341-1348

KNAUST, D., 2009. Characterisation of a Campanian deep-sea fan system in the Norwegian Sea by means of ichnofabrics. Marine and Petroleum Geology, 26(7), pp. 1199-1211

KVILHAUG, T. and ROALDSET, E., 1998. Rock mechanical characterization of an offshore mudrock from Haltenbanken, Mid-Norway. Rock Mechanics and Rock

Engineering, 31(2), pp. 95-115

LANCASTER, S. and WHITCOMBE, D., 2000. Fast-track 'coloured' Inversion. Society of Exploration Geophysicists.

LANG, W.H., 1994. Compaction/Diagenesis of Sediments and Compaction Gradients in Relation to Interval Transit Time. Society of Petrophysicists and Well-Log Analysts.

LAURENT, D., GAY, A., BAUDON, C., BERNDT, C., SOLIVA, R., PLANKE, S., MOURGUES, R., LACAZE, S., PAUGET, F., MANGUE, M. and LOPEZ, M., 2012. High-resolution architecture of a polygonal fault interval inferred from geomodel applied to 3D seismic data from the Gjallar Ridge, Vøring Basin, Offshore Norway. Marine Geology, 332–334, pp. 134-151

MANUEL COBOS, C. and CASTAGNA, J., 2014. Stochastic Rock Physics Inversion. - International Petroleum Technology Conference.

MAVKO, G., MUKERJI, T. and DVORKIN, J., 2009. The Rock Physics Handbook. Cambridge: Cambridge University Press.

MINDLIN, R.D., 1949. Compliance of Elastic Bodies in Contact. Journal of Applied Mechanics-Transactions of the Asme, 16(3), pp. 259-268

MORTON, A.C., WHITHAM, A.G. and FANNING, C.M., 2005. Provenance of Late Cretaceous to Paleocene submarine fan sandstones in the Norwegian Sea: Integration of heavy mineral, mineral chemical and zircon age data. Sedimentary Geology, 182(1–4), pp. 3-28

MOYANO, B., JENSEN, E.H. and JOHANSEN, T.A., 2015. Spatial constrained inverse rock physics modelling. Geophysical Prospecting, 63(1), pp. 183-191 MSOLO, A. and GIDLOW, M., 2015. Relative Rock Physics Templates in the Elastic Impedance Domain. Society of Exploration Geophysicists.

ONAJITE, E., 2014. Chapter 1 - Sedimentation and Oil/Gas Formation. In: E. ONAJITE, ed. Seismic Data Analysis Techniques in Hydrocarbon Exploration. Oxford:

Elsevier. pp. 3-16

ONAJITE, E., 2014. Chapter 14 - Understanding Reflection Coefficient. In: E. ONAJITE, ed. Seismic Data Analysis Techniques in Hydrocarbon Exploration. Oxford: Elsevier. pp. 213-228

RAMM, M. and BJORLYKKE, K., 1994. Porosity Depth Trends in Reservoir Sandstones - Assessing the Quantitative Effects of Varying Pore-Pressure, Temperature History and Mineralogy, Norwegian Shelf Data. Clay Minerals, 29(4), pp. 475-490

RAVNÅS, R., COOK, A., ENGENES, K., GERMS, H., GRECULA, M., HAGA, J., HARVEY, C. and MACEACHERN, J.A., 2014. The Ormen Lange turbidite systems. From Depositional Systems to Sedimentary Successions on the Norwegian Continental Margin. John Wiley Sons, Ltd. pp. 609-645

RUSSELL, B., HAMPSON, D. and BANKHEAD, B., 2006. An Inversion Primer. CSEG Recorder, 31(Special), pp. 96

SAIN, R., MAVKO, G. and MUKERJI, T., 2009. Effect of diagenesis on Elastic and Transport Properties using Computational Rock Physics in realistic pore microstructure. Society of Exploration Geophysicists.

SERRA, O., 2008. Well Logging Handbook. Editions Technip.

SETOYAMA, E., RADMACHER, W., KAMINSKI, M.A. and TYSZKA, J., 2013. Foraminiferal and palynological biostratigraphy and biofacies from a Santonian–Campanian submarine fan system in the Vøring Basin (offshore Norway). Marine and Petroleum Geology, 43(0), pp. 396-408

SHANMUGAM, G., LEHTONEN, L.R., STRAUME, T., SYVERTSEN, S.E., HODGKINSON, R.J. and SKIBELI, M., 1994. Slump and Debris-Flow Dominated Upper Slope Facies in the Cretaceous of the Norwegian and Northern North Seas (61-67-Degrees-N) - Implications for Sand Distribution. Aapg Bulletin-American Association of Petroleum Geologists, 78(6), pp. 910-937

SHUEY, R.T., 1985. A Simplification of the Zoeppritz Equations. Geophysics, 50(9),

pp. 609–614-1522

SIMM, R., 2007. Practical Gassmann fluid substitution in sand/shale sequences. First Break, 12(25),

SIMM, R. and BACON, M., 2014. Seismic Amplitude An Interpreter's Handbook. Cambridge University Press.

THOMOPOULOS, N.T., 2013. Essentials of Monte Carlo Simulation - Statistical Methods for Building Simulation Models. New York: Springer.

TIAB, D. and DONALDSON, E.C., 1996. Petrophysics - Theory and Practice of Measuring Reservoir Rock and Fluid Transport Properties (2nd Edition). Elsevier.

WANG, C., WANG, Y., WANG, X. and XUN, C., 2016. Multicomponent seismic noise attenuation with multivariate order statistic filters. Journal of Applied Geophysics, 133, pp. 70-81

WANG, Z., WANG, H. and CATES, M., 2001. Effective elastic properties of solid clays. Geophysics, 66(2), pp. 428-440

WESTPHAL STEPHENSEN, M., LARSEN, M., DAM, G. and HANSEN, T., 2013. The Glenlivet gas discovery – an integrated exploration history. First Break, 31(7), pp. 51-64

WHITCOMBE, D.N., CONNOLLY, P.A., REAGAN, R.L. and REDSHAW, T.C., 2000. Extended Elastic Impedance For Fluid And Lithology Prediction. Society of Exploration Geophysicists.

WHITE, R., SIMM, R. and XU, S.Y., 1998. Well tie, fluid substitution and AVO modelling: A North Sea example. Geophysical Prospecting, 46(3), pp. 323-346 YIN XINGYAO, ZONG ZHAOYUN and WU GUOCHEN, 2015. Research on seismic fluid identification driven by rock physics. Science China-Earth Sciences, 58(2), pp. 159-171

Appendix A - Interpretation Sections

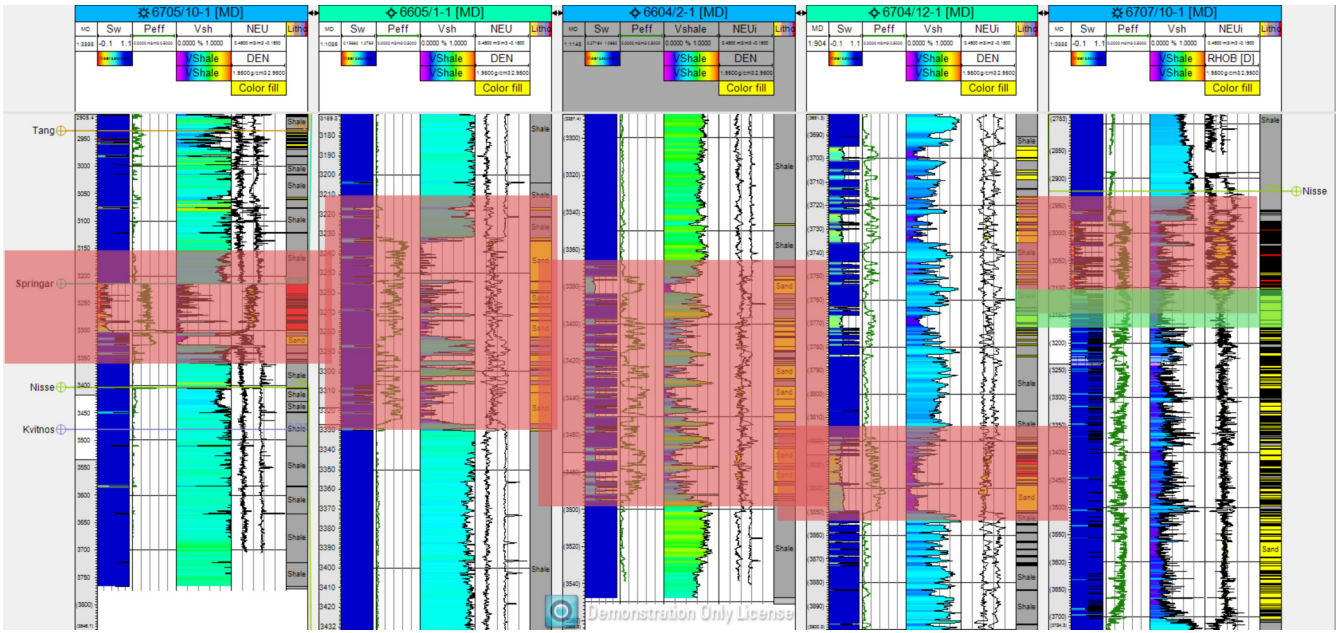

Figure 6.1: Cross Sections of wells showing location of reservoirs

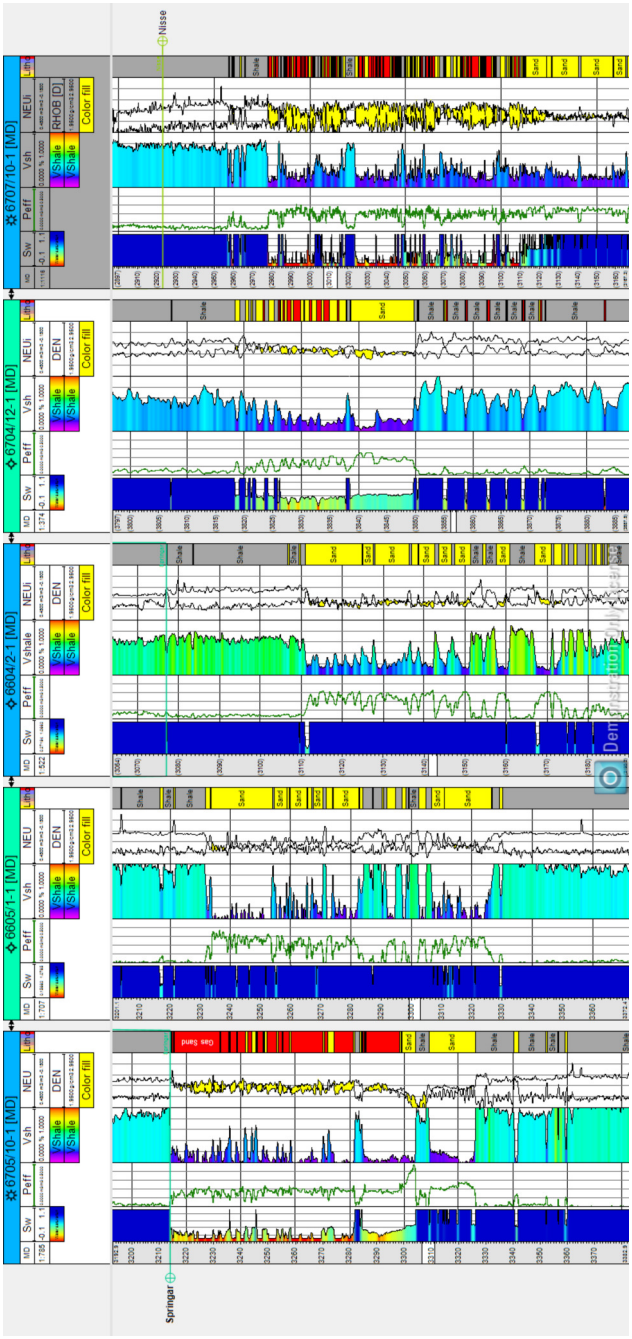

Figure 6.2: Cross Sections of calculated logs

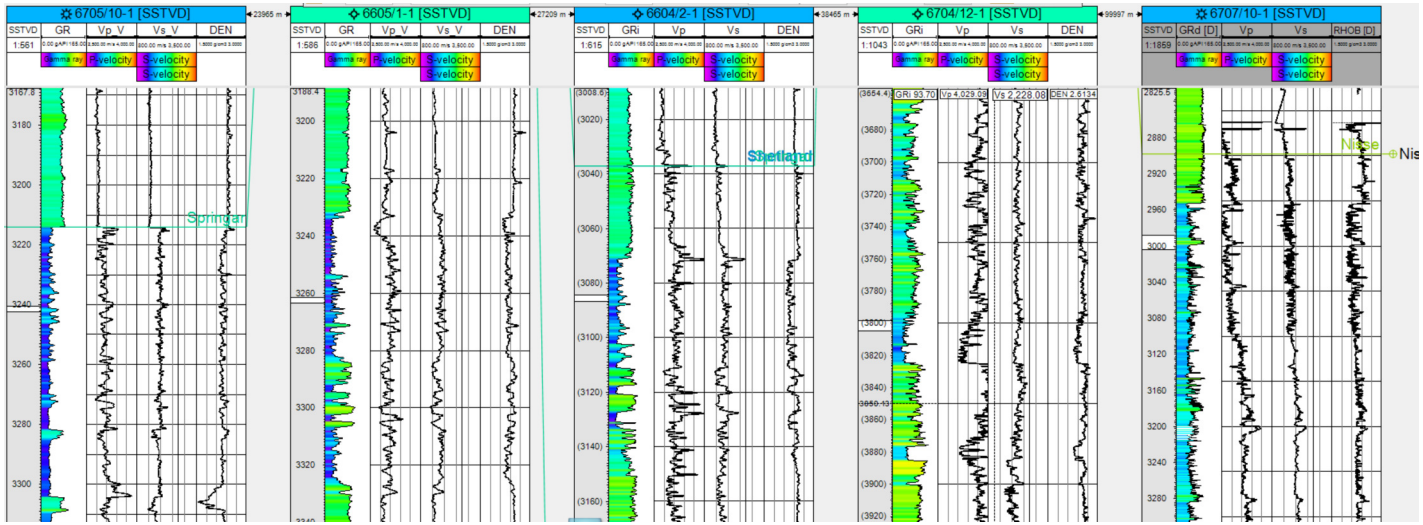

Figure 6.3: Cross Sections of geophysical logs

Appendix B - Fluid Substitution Equations

Gassman Equation

1. Estimate Bulk Modulus and Density for original and new fluids

    2. Estimate the bulk modulus and density of the solid $K_0 Rho_0$

    3. Calculate original saturated moduli K (6.1) + G (6.2)

$$K = RhoVp^2 - \frac{4}{3}Vs \tag{6.1}$$

$$G = RhoVs^2 \tag{6.2}$$

    4. Calculate K_{dry}6.3

$$K_{dry} = \frac{K(\frac{\Phi K_0}{K_f} + 1 - \Phi) - K_0}{\frac{\Phi K_0}{K_f} + \frac{K}{K0} - 1 - \Phi} \tag{6.3}$$

    5. Calculate $K_{sat} fornewfluid$(6.4)

$$K = K_{dry} + \frac{(1 - \frac{K_{dry}}{K_0})^2}{\frac{\Phi}{K_f} + \frac{1-\Phi}{K_0} - \frac{K_{dry}}{K_0^2}} \tag{6.4}$$

    6. Calculate Density (6.5)

$$Rho = Rho_0 - ((\Phi - Rho_{fl1}) - (\Phi - Rho_{fl2})) \tag{6.5}$$

7. Calculate new Vp and Vs

Mixing Methods

The mixing methods define the Bulk or Shear modulus for a mixture of two elements. In this case of this study it is a mixture of sand and shale based on the value of the VShale curve which is used to calculate the real Bulk and Shear modulus.

$$Mv = AM_A + (1 + A)M_B$$

Voight Upper Bound calculation for a 2 phase mixture

$$\frac{1}{M_R} = \frac{A}{M_A} + \frac{(1 - A)}{M_B}$$

Reuss Lower Bound calculation for a 2 phase mixture

$$M_(VRH) = \frac{M_V + M_R}{2}$$

Hill Average for a 2 phase mixture